Metal–Nonmetal Transition in Metal–Ammonia Solutions via the Inhomogeneous Transport Regime[1]

Morrel H. Cohen*

The James Franck Institute and Department of Physics, The University of Chicago, Chicago, Illinois 60637

and Joshua Jortner

Department of Chemistry, Tel-Aviv University, Tel-Aviv, Israel *(Received July 23, 1975)*

In this paper we present a coherent physical picture of the metal–nonmetal transition in metal–ammonia solutions in the intermediate concentration range. We propose that in Li–NH_3 and Na–NH_3 solutions at $T - T_c \simeq 10$–20 K the metallic propagation regime (9–16 MPM) is separated from a nonmetallic pseudointrinsic semiconducting regime (1–2.3 MPM) by a microscopically inhomogeneous regime (2.3–9 MPM) in which the concentration fluctuates locally about either of two well-defined values M_0 and M_1, $M_0 > M_1$, the local concentration remaining near M_0 or M_1 over radii approximately equal to the Debye short correlation length, b, for concentration fluctuations. The limits of the inhomogeneous regime were determined from a combination of concentration fluctuation measurements, electrical conductivity, Hall effect, and paramagnetic susceptibility data to be $M_0 = 9$ MPM and $M_1 = 2.33$ MPM, which yield the C scale, $C = (M - 2.33)/6.66$, for both Li–NH_3 at 223 K and for Na–NH_3 at 240 K. We have also established the consistency of our picture with the available magnetic data for Na solutions. An analysis of electronic transport, thermal transport, optical properties, and sound velocity was carried out in terms of a theory of response functions for microscopically inhomogeneous materials developed by us. Excellent agreement between theory and experiment was obtained throughout the entire inhomogeneous transport regime.

I. Introductory Remarks

In this paper we present a physical picture for the metal–nonmetal transition (MNMT) in metal–ammonia solutions (MAS) in the intermediate concentration range (1–10 MPM).[2-5] The apparently continuous changes of the electronic and thermal transport properties as well as the optical data and thermochemical properties of MAS in the intermediate concentration range provide an important example of a MNMT in a disordered material. Many examples for such MNMT in disordered solids and liquids are now well documented.[6] What is a MNMT in a disordered material? From the point of view of the experimentalist such "transitions" may be roughly classified in terms of the variation of the electrical conductivity, σ, induced by changes in a primary variable of state, such as density in a one-component system or composition in a two-component system:

1. "Abrupt" MNMT. A sharp drop of σ is exhibited in a narrow range of the primary variable of state. We are aware of a single example of such a transition which was observed[7] in amorphous films of Cu–Ar and Pb–Ar at 4 K. σ decreases gradually over the composition range 100–60 mol % metal, exhibiting a "discontinuity" at about ~55 mol % metal. We note in passing that the percolation picture[8-13] which implies that

$$\sigma = 0;\ C < C^*$$

$$\sigma \propto (C - C^*)^{1.6};\ C^* < C < 0.4$$

$$\sigma \propto \left(\frac{3}{2}C - \frac{1}{2}\right);\ 0.4 < C < 1 \qquad \text{(I.1)}$$

where C is the metallic volume fraction and $C^* \simeq 0.17$ is the percolation threshold,[12,13] also provides at least a semiquantitative fit of these experimental data.

2. "Continuous" MNMT. A gradual variation of σ is observed. Many such cases have been recorded in disordered materials. To quote several illustrative examples we mention the MNMT in expanded liquid metals[14-25] and in MAS.[2-5,26-48] Such MNMT's were studied at finite temperatures, and one can argue that thermal excitations will erode any discontinuity in σ.

Two basic theoretical models for the MNMT were advanced by Mott[6,49-57] which rest either on (a) correlation effects or (b) band overlap effects. Mott further invokes the central role of Anderson localization and of polaron effects in determining the features of the MNMT in disordered materials. An alternative model was advanced by the present authors (CJ)[58-63] who argued that in many disordered materials the MNMT occurs via an inhomogeneous transport regime, where microscopic inhomogeneities, e.g., density fluctuations, bonding modifications, or concentration fluctuations, determine the electronic structure and the transport properties. Thus in the CJ approach mechanisms a or b operate *locally*. Mott's picture implies the occurrence of a discrete MNMT at 0 K, while CJ assert that in a disordered material which is characterized by a large correlation length for fluctuations, or by large potential fluctuations, a continuous MNMT will be exhibited. The CJ picture is necessary to overcome serious difficulties encountered in the interpretation of the transport properties of many disordered materials undergoing a MNMT in terms of conventional descriptions of transport mechanisms.

II. Conventional Descriptions of Disordered Metals and Nonmetallic Materials

We wish to understand the nature of the apparently continuous changes of electronic structure and transport properties during the course of a transition from metallic to nonmetallic behavior in disordered systems and in particular in MAS. Let us first characterize the general features of disordered metals and disordered nonmetallic materials in terms of their transport properties. One can specify the transport properties of disordered metals in terms of one of the following transport regimes.

(a) The Metallic Propagation Regime.[64] The mean free path of the conduction electrons considerably exceeds the Fermi wavelength $\lambda_F = k_F^{-1}$, i.e. $l \gg \lambda_F$. The conductivity σ is well represented by the nearly free-electron theory.[64,65] There is no special relation between the Hall coefficient, R, and the conductivity.[66,67] On experimental and theoretical[67] grounds we assert that the latter quantity is close to the free-electron value, R_{FE}, whereupon the Hall mobility $\mu = \sigma R$ is dominated by changes in σ. Correspondingly, the transport properties satisfy the conditions

$$\sigma \gtrsim 3000\ (\Omega\ \text{cm})^{-1} - 1000\ (\Omega\ \text{cm})^{-1} \tag{II.1a}$$

$$R \simeq R_{FE} \tag{II.1b}$$

$$\mu = R\sigma \simeq R_{FE}\sigma \tag{II.1c}$$

A minimum value of $\sim$1000 $(\Omega\ \text{cm})^{-1}$ for the conductivity in the propagation regime is applicable to MAS, where the electron density is low.

(b) The Metallic Diffusion Regime.[50,68-71] As disorder increases the mean free path decreases to a point where $l \sim \lambda_F$. The concept of a mean free path is no longer applicable. However, in the propagation regime l characterizes the distance over which the electronic wave functions retain phase coherence. We can generalize l into a phase coherence length, which can be arbitrarily small. For $l < \lambda_F$ the phase of the electronic wave functions becomes effectively random and interference effects are unimportant. The random phase approximation is applicable within the framework of the Kubo–Greenwood formalism in this problem. Friedman[70] has studied transport in a crystal with a tight-binding s band. He assumes that the wave function amplitudes are everywhere constant but the phases on different sites are random. An extension of this treatment has been provided by Varea de Alvarez and Keller.[72] Friedman's treatment[70] results in

$$\sigma = \frac{2\pi}{3} Z \left(\frac{e^2}{\hbar a}\right) X^2$$

$$R \simeq Z^{-1} R_{FE} X^{-1}$$

$$\mu \simeq \frac{2\pi}{3} \left(\frac{ea^2}{\hbar}\right) X \tag{II.2}$$

where a is the internuclear separation, or the intercavity spacing in MAS, z is the number of nearest neighbors, and the parameter

$$X = Ja^3 n(E_F) \tag{II.2a}$$

contains J, the nearest neighbor electron transfer integral and the density of states, $n(E_F)$, at the Fermi energy E_F. Two conclusions are immediately apparent. First, the variation of the conductivity in the diffusion regime induced by changes in a primary variable of state is not only determined by the changes of $n(E_F)$ but can be also considerably affected by the changes of J. Thus the Mott relation[51-53] $\sigma = A[n(E_F)]^2$, where $A \sim 2500\ (\Omega\ \text{cm})^{-1}$ and $n(E_F)$ is extracted from the Knight shift or the paramagnetic susceptibility for the conductivity in the diffusion regime, is of limited applicability. Second, one can derive explicit relations between the Hall coefficient and other electrical transport properties

$$\sigma \propto (R_{FE}/R)^2$$

$$\mu \propto (R_{FE}/R) \tag{II.3}$$

where the proportionality factors contain parameters which depend either explicitly or weakly on the variable of state. These relations provide an important diagnostic tool for the identification of diffusive or Brownian motion, i.e., the strong scattering regime.

Turning to nonmetallic materials we consider the most common case, that of disordered semiconductors, where there are two transport mechanisms in parallel.

(c) Pseudointrinsic Semiconductivity. In the current picture of disordered semiconductors the band gap is replaced by a mobility gap[69,51,52,73]

$$E_g = E_c - E_v \tag{II.4}$$

where E_c and E_v correspond to the mobility edges in the conduction band and in the valence band, respectively. All the states within the mobility gap are localized, and $\sigma = 0$ at $T = 0$. Conduction at sufficiently high temperatures proceeds by thermal excitation of carriers across the mobility gap. The conductivity is[69,73]

$$\sigma \simeq \sigma(E_c) \exp[-(E_c - E_F)/kT]$$

$$\sigma(E_c) = 2n(E_c) e\mu(E_c) kT \tag{II.5}$$

where $n(E_c)$ and $\mu(E_c)$ are the density of states and the (mean) mobility near the mobility edge, respectively. To derive a relation between the conducitivity and the thermoelectric power, S, Mott and Cutler started from the relations[74]

$$\sigma = -\int \sigma(E)(\partial f/\partial E)\, dE \tag{II.6}$$

$$S\sigma = \frac{k}{e} \int \sigma(E) \left(\frac{E - E_F}{kT}\right) (\partial f/\partial E)\, dE \tag{II.7}$$

where f is the Fermi distribution function. Assuming that $\sigma(E)$ is weakly dependent on E above E_c, these formula give

$$\sigma \simeq \sigma(E_c) f(E_c) \tag{II.8}$$

which is practically identical with eq I.5, and

$$S = \frac{k}{e} \{\ln (\sigma(E_c)/\sigma) + [1 + (\sigma(E_c)/\sigma)] \ln [1 + (\sigma/\sigma(E_c))]\} \tag{II.9}$$

when one band dominates. When $\sigma/\sigma(E_c) \ll 1$, i.e. $E_c - E_F > 4kT$, eq I.9 reduces to the conventional form

$$S = \frac{k}{e} [\ln (\sigma(E_c)/\sigma) + 1] \tag{II.10}$$

The σ vs. S relations (II.9) and (II.10) unambiguously specify pseudointrinsic semiconductivity, provided that compensation effects do not affect S.

(d) Pseudoextrinsic Semiconductivity. In general, the Fermi energy is located within the mobility gap and $n(E_F)$ is finite. Consequently, electrons near the Fermi energy

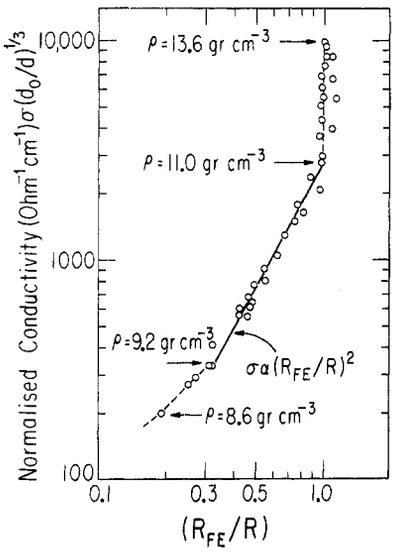

Figure 1. The dependence of the electrical conductivity on R_{FE}/R for expanded liquid Hg, after Even and Jortner (ref 20). The diffusion regime spans the density range 9.3 g cm^{-3} < ρ < 11.0 g cm^{-3}, $\sigma \propto (R_{FE}/R)^2$ in accordance with eq II.3.

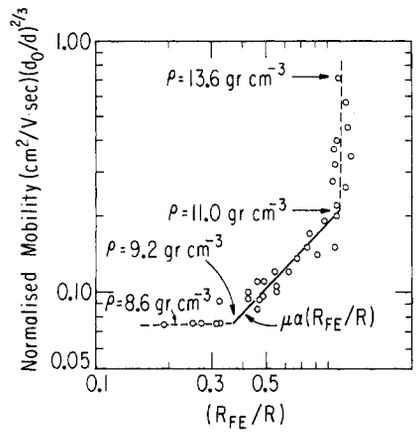

Figure 2. The dependence of the Hall mobility on $(R_{FE}/R)^2$ for expanded liquid Hg, after Even and Jortner (ref 20). In the diffusion regime 9.3 g cm^{-3} < ρ < 11.0 g cm^{-3}, $\mu \propto (R_{FE}/R)$ in agreement with eq II.3.

contribute to the transport via variable range hopping.[54,75] At sufficiently low temperatures this Mott hopping will dominate the conductivity. The thermopower[76] is expected to be small and not related to σ. This mechanism is important only at low temperatures, and we shall not be concerned with it here.

In MAS an additional transport regime is exhibited.

(e) Electrolytic transport regime where conventional electrolytic transport[4] prevails. According to Mott's picture the MNMT in a disordered system will be manifested by an "abrupt" switching of the transport mechanisms from regime b (or regime a) to semiconducting transport (mechanisms c and d) in materials undergoing a metal–semiconductor transition such as expanded liquid Hg. In MAS a switch from regime b to regime e may be exhibited, or alternatively the transition from regime b to regime c will occur. As several of these conventional transport regimes have already been identified[55,56,59,70] in expanded liquid Hg we proceed to the analysis of the experimental evidence for this relatively simple one-component system.

III. Transport in Expanded Liquid Mercury

For expanded liquid Hg the extensive experimental data[14-24] for σ, R, and S over the density range 13.6–5 g cm^{-3} can be partially understood in terms of the following distinct transport regimes: (a) propagation regime, 11 g cm^{-3} < ρ < 13.6 g cm^{-3} where eq II.1 applies, as is evident from the data of Even and Jortner reproduced in Figures 1 and 2; (b) diffusion regime, 9.2 g cm^{-3} < ρ < 11.0 g cm^{-3} where Friedman's relations, eq II.3, apply (Figures 1 and 2); and (c) pseudointrinsic semiconducting regime, ρ < 7.8 g cm^{-3} where the ln σ vs. S relation, eq II.10, holds. In the intermediate density range ρ = 9.2–7.8 g cm^{-3} the electrical conductivity[14-18] at 1550°C varies in the range 500–20 (Ω cm)$^{-1}$, the Hall mobility μ (which was measured down to 8.6 g cm^{-3}) is practically constant,[20] μ = 0.07 cm^2 V^{-1} sec^{-1}, the thermoelectric power[18] exhibits a weak variation with ρ, S = −70 (μV/°C) at ρ = 9.2 g cm^{-3} and S = −150 (μV/°C) at 7.8 g cm^{-3}, while the volume and temperature dependence of σ reveal a fast increase with decreasing density.[16,18] None of the conventional transport regimes appears to be consistent with the transport data in this intermediate density range, in our opinion. However, Mott's picture[55,56] for the metal–nonmetal transition in Hg asserts that the material remains microscopically homogeneous with regard to electronic structure and transport. When the density of states ratio g falls below a critical value $g^* \simeq 1/3$, Mott supposes the states to be localized. Accordingly, he proposes that a mobility gap opens at ρ = 9.2 g cm^{-3}, and that for lower densities the transport properties are determined by excitation to the mobility edge, the conductivity being given by eq 1.5. Mott's model encounters three serious difficulties. First, it was argued by Mott[56] that in this model μ is given by the Hall mobility of electrons at the mobility edge and is thus expected to be practically independent of density, in agreement with experiment. However, it should be noted that according to the Friedman theory[70] for the Hall mobility in an amorphous semiconductor $\mu \propto Jn(E_c)$ where $n(E_c)$ is the density of states at the mobility edge. Thus both in the metallic diffusion regime (see, e.g., (II.2)) and in the semiconducting regime the variation of the conductivity and of the Hall mobility with decreasing density will be strongly affected by the decrease of the transfer integral J with decreasing ρ. Thus the Hall mobility is not expected to remain constant throughout the semiconducting regime in expanded Hg. Second, Mott's approach leads to a substantial disagreement between the density variation of the electrical conductivity and the thermoelectric power in the intermediate density range. A recent analysis of the thermoelectric power data of Schmutzler and Hensel[18] demonstrates that eq I.9 and I.10 are not obeyed for Hg in the intermediate density range. If we assume that the mobility gap opens up (i.e., $E_c - E_F$ = 0) at 9.2 g cm^{-3} and reaches $4kT$ at 7.8 g cm^{-3}, the highest density for which eq II.10 is obeyed, we have to take $\sigma_M = \sigma$ (9.2 g cm^{-3}) = 550 (Ω cm)$^{-1}$. As is evident from Figure 3, eq II.9 results in a much weaker decrease of σ/σ_M with increasing $|S|$ than is experimentally observed in the intermediate density range. Any other choice of σ_M will not reproduce the experimental σ vs. S relation for 7.8 g cm^{-3} < ρ < 9.2 g cm^{-3}. Thus the discrepancy is a serious one. To overcome this difficulty Mott has recently suggested[56] an additional contribution to the thermoelectric power in the semiconducting range for $E_c - E_F > kT$ which originates from a negative heat of transport. We note in passing that in order

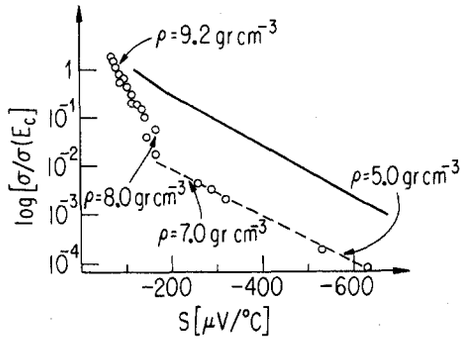

Figure 3. The dependence of ln σ on S for expanded liquid Hg, after Schmutzler and Hensel (ref 18). The solid line represent Mott's analysis (eq II.9). The dashed line corresponds to a slope of (k/e). According to eq II.10 the pseudointrinsic semiconducting regime holds for $\rho < 7.8$ g cm^{-3}.

to provide a quantitative fit of the experimental data Mott had to invoke[56] a change of the negative heat of transport, ΔH, from zero at 9.2 g cm^{-3} to −0.25 eV at 7.8 g cm^{-3}, which is half the energy gap. It is rather difficult to comprehend how the polaron effects proposed by Mott can be operative in a small-gap semiconductor at high temperatures where $4kT > |\Delta H|$. Third, we have pointed out[59] that the density dependence of $E_c - E_F$ which can be extracted from Mott's picture, together with basic thermodynamic considerations concerning the amplitude of the density fluctuations, inevitably leads to the conclusion that the conductivity is nonuniform over distances L which considerably exceed the phase coherence length l for the conduction electrons. For the average density $\rho = 8.5$ g cm^{-3} we find $\Delta\sigma/\sigma_{mode} = 2.7$ for $L = 15$ Å and $\Delta\sigma/\sigma_{mode} = 0.5$ for $L = 40$ Å, where σ_{mode} and $\Delta\sigma$ are the most probable conductivity and the spread of the distribution. Thus if we start with a homogeneous material we inescapably wind up with nonuniformity. We thus conclude that Mott's model[55,56] does not provide a self-consistent picture for the variation of the electrical and thermal transport properties in the intermediate density range. In other words, the conventional transport regimes, which assume microscopic homogeneity of the material, appear to be inconsistent with the data in this density range.

We have proposed[59] that the electronic structure and transport properties of expanded liquid Hg in the density range 9.2–8.0 g cm^{-3} are intermediated by density fluctuations. Invoking a unimodal distribution for the density fluctuations, as appropriate for a density range where the Ornstein–Zernicke decay length is of the order the interatomic spacing, we were able to provide a coherent physical picture for the continuous metal–nonmetal transition in this system. In that process we have established[59] the volume fraction, C, of the metallic regions (where the s–p band gap did not open locally). This C scale should be regarded as a theoretical prediction of the Knight shift and paramagnetic susceptibility throughout the inhomogeneous transport regime. The recent Knight shift data of El-Hamary and Warren[77] in the density range 9.2–8.0 g cm^{-3} are in excellent agreement with our predictions.

IV. Transport in MAS

We now turn to the central issue of the present paper and consider the identification of conventional transport regimes in MAS. In concentrated MAS (20–10 MPM), Lepoutre[78] and Thompson[79] find that $l = 70$ Å and $k_F = 0.49$ Å^{-1} at 20 MPM decreasing to $l = 12$ Å and $k_F = 0.40$ Å^{-1} at 10 MPM, so that the basic condition for the propagation of conduction electrons between scattering events, $k_F l \geq 3$, is satisfied down to about 10 MPM. For expanded liquid Hg the propagation regime terminates at $k_F l = 2.3$. Thus for concentrated (10–20 MPM) MAS solutions, the propagation regime applies. The decrease of σ with dilution in the propagation regime can be well accounted for in terms of the NFE model and is primarily a consequence of the concentration dependence of the structure factors and the increase of the fraction of unbound ammonia molecules.[80,81] The Hall coefficient[32–35] is $R = R_{FE}$, and the variation of μ is dominated by the changes in σ as expected for the propagation regime.

In the intermediate concentration regime (2–10 MPM), the Friedman relations (II.3) do not hold. (R_{FE}/R) changes only from 1.0 to 0.5. However, σ decreases by three orders of magnitude and μ by two orders of magnitude, so that (R_{FE}/R) should decrease from 1.0 to 0.03 in that concentration range according to the Friedman relations.[70] One could instead attempt to establish whether the conductivity relation (II.2) does hold. From an analysis of the experimental conductivity and volume susceptibility χ_p in this concentration range we have established that $\sigma = A\chi_p^{2.3}$. This power is not so different from the value of 2.0, expected by Mott, however, in the concentration range 10–2 MPM the transfer integral $J \propto \exp[-\beta a]$, where[82] $\beta \sim 0.55$ Å^{-1}, decreases by one order of magnitude due to the decrease of a by a factor of ~2. Thus the correct version of the conductivity relation in the diffusion regime $\sigma \propto \chi_p^2 \exp[-2\beta a]$ does not hold. We thus conclude that the physical properties of MAS in the intermediate region cannot be accounted for in terms of a diffusion type of metallic transport, and that the MNMT in this system is not preceded by a homogeneous diffusion regime as does happen in expanded liquid Hg. The conductivity in the intermediate regime $\sigma = 10^3 - 1$ (Ω cm)$^{-1}$ is so high that it cannot be assigned to semiconducting transport (mechanism c, section II). Furthermore, relations (II.9) and (II.10) do not hold in this range. Obviously, the electrolytic transport regime ((e), section II) also does not apply. Thus none of the conventional transport regimes is applicable in the concentration range from ~2 to ~10 MPM.

We now turn to a brief summary of the transport properties at lower concentrations.[4] At $M \simeq 10^{-1}$ MPM the equivalent conductance, Λ_e, goes through a minimum. It has been suggested that the increase of Λ_e with increasing M is associated with the onset of electronic conduction. For this to occur, spin depairing must be observed. The spin susceptibility reaches a low value $\chi_p \simeq 0$ at 1 MPM and increases slowly in the range 1–2.3 MPM. We thus prefer a physical picture where dissociation of neutral quartets (i.e., $2M^+ 2e^-$) into negative spin paired triplets ($M^+ 2e^-$) and positive ions prevails in the concentration range from 10^{-1} to 1 MPM resulting in an increase of Λ_e, so that the conventional electrolytic transport regime prevails up to at least 0.5 MPM. One can roughly estimate an upper limit to Λ_e expected when dissociation is complete. Coulomb effects, as in the Onsager–Fuoss theory, act so as to reduce the equivalent conductance below its limiting value 760 (Ω mol)$^{-1}$. The latter is, therefore, an upper limit. The equivalent conductance at 0.5 MPM is[4] 550 (Ω mol)$^{-1}$ indicating that dissociation is substantial, if not complete, at that concentration. At 1 MPM $\Lambda_e = 770$ (Ω mol)$^{-1}$ and electrolytic transport cannot account for the conductivity above that

TABLE I: Assignments of Conventional Transport Regimes in MAS[a]

M, MPM	Transport regimes	Experimental evidence
16–9	Metallic propagation	$\sigma = 5 \times 10^3 - 10^3$ $(\Omega\ \text{cm})^{-1}$ $R = R_{FE}$ $l \simeq 70$–12 Å Applicability of (RMP) Thermal transport and optical properties
9–2.3	?	$\sigma = 10^3 - 1$ $(\Omega\ \text{cm})^{-1}$ $R/R_{FE} = 1$–2 Inapplicability of (FR)
2.3–1	Disordered semiconductor	$\sigma = 0.16 - 1$ $(\Omega\ \text{cm})^{-1}$ $\chi_p = 0$ at 1 MPM to $\sim 8 \times 10^{-8}$ cgs at 2.3 MPM
<0.5	Electrolytic	$\Lambda_e < 550$ $(\Omega\ \text{mol})^{-1}$

[a] M–NH_3 liquid; $T - T_c \sim 10$–20 K; for Li, Na–NH_3. RMP = relations for metallic propagation regime, eq 11.1. FR = Freedman relations for metallic diffusion regime, eq 11.3.

concentration. We suggest that in the concentration range from ~1 to ~2 MPM an electronic transport mechanism sets in. As at ~1 MPM complete spin pairing occurs, we suggest a pseudointrinsic semiconducting transport (mechanism c, section II) to be operative in MAS in the range ~1–2 MPM. The full valence band corresponds to doubly occupied σ_g-type orbitals of electron cavity pairs within triplets. The conduction band consists of a superposition of σ_u-type orbitals. The low density band gap corresponding to the σ_g–σ_u excitation within a single cavity pair is 0.6–0.7 eV. Thus electronic structure and transport in MAS in the latter region are analogous to those exhibited in semiconducting expanded Hg for $\rho < 7.8$ g cm^{-3}.

The present status of our efforts to identify the conventional transport regimes in MAS undergoing a "continuous" MNMT is summarized in Table I. None of the conventional transport regimes is applicable in the intermediate (2.3–9 MPM) concentration range. We have proposed that in Li–NH_3 and Na–NH_3 solutions the metallic propagation regime is separated from a nonmetallic (semiconducting) regime by a microscopically inhomogeneous regime in which concentration fluctuations determine electronic structure and transport properties in this two-component system. We now proceed to a semiquantitative exploration of the effects of microscopic density fluctuations on the electronic properties of MAS.

V. Microscopic Inhomogeneities in MAS

We propose that the metal–nonmetal transition in MAS is intermediated by concentration fluctuations. In the present context the three major questions concerning the fluctuations are: (a) the spatial extent of fluctuations; (b) whether they are of large amplitude; and (c) whether they are unimodally or multimodally distributed. Let us consider the local value $m(r)$ of a configurational parameter which could refer to the local density in a one-component system or to the local concentration in a multicomponent system. The mean value of the configurational parameter is $\langle m(\vec{r})\rangle = M$ while the autocorrelation function, $A(R)$, is

$$A(R) = \frac{\langle m(\vec{r}+\vec{R})m(\vec{r})\rangle - M^2}{M^2} \qquad \text{(V.2)}$$

Condensed systems are stiff, tending to resist rapid change in local configuration so that, roughly speaking, $m(\vec{r})$ varies significantly over distances greater than b, the short correlation length. For liquids we know from the Ornstein–Zernike theory for fluctuations that the asymptotic decay of $A(R)$ is exponential. We can set

$$A(R) \approx \text{constant} \qquad R < b$$
$$A(R) \sim \exp(-R/\zeta)/R \qquad \text{(V.3)}$$

where ζ is the fluctuation decay length. Provided that $b \gg a$ and $b > \zeta$ the values of $m(\vec{r})$ at two points separated by more than b are statistically independent. We can then idealize the physical picture, replacing $A(R)$ by a simple step function

$$A(R) = \text{constant} \qquad R \leq b$$
$$A(R) = 0 \qquad R > b \qquad \text{(V.4)}$$

b thus specifies the spatial extent of the fluctuations. The rms amplitude of the fluctuations is determined by $A(R < b)$. Two examples of the probability distribution $P(m(\vec{r}))$, of the local values of $m(\vec{r})$ are given in Figure 4.

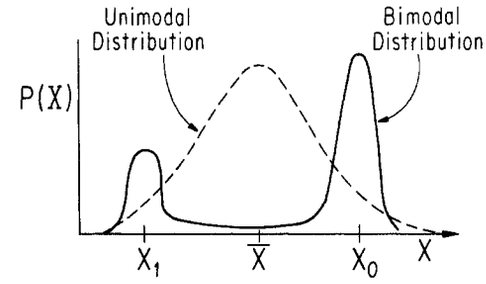

Figure 4. Examples of the probability distribution $P(X(\vec{r}))$ of the local values of the primary variable of state.

There are several experimental techniques available to probe the nature of microscopic inhomogeneities in disordered materials. The spatial extent of fluctuations can be monitored by small angle x-ray and neutron scattering, or by electron microscopy and diffraction. The amplitudes of the fluctuations can be inferred from structure factors, ultrasonic attenuation, and determinations of concentration fluctuations through chemical potential measurements in a multicomponent system. No direct evidence is currently available concerning the probability distribution function $P(m)$ for the local concentration in a two-component liquid. It should be emphasized at this point that the proposed microscopic inhomogeneities are distinct from critical fluctuations; a careful examination of the experimental data is required to separate these two physical effects. We now proceed to explore the nature of microscopic inhomogeneities and consider the experimental evidence for them in MAS.

There is substantial evidence for large amplitude concentration fluctuations in metal–ammonia solutions. Thompson and Ichikawa[83] have found direct evidence for large concentration fluctuations in lithium and sodium ammonia solutions, but not in cesium solutions. They measure the dependence of the chemical potential of the metal on metal concentration at −33 K and from it extract the mean square concentration fluctuation in the form $\langle(\Delta X_M)^2\rangle$ where ΔX_M is the fluctuation of the mole fraction. Their results are shown in Figures 5–7. Li and Na solutions saturate at 20 and 16 MPM, respectively;[4] the Cs solutions do not saturate.[84] In Figures 5–7 we compare the observed fluctuations with those expected from an ideal mixture of NH_3 and $M(NH_3)_n$, with $n = 4$ for Li and 6 for Na and Cs.

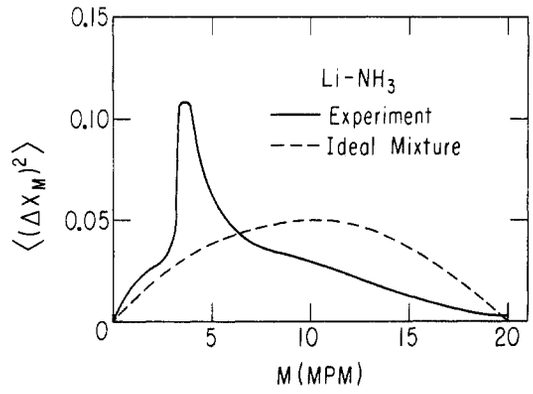

Figure 5. Mean square of concentration fluctuations in Li–NH_3 solutions: solid lines, experimental data (ref 83); dashed line, ideal mixture.

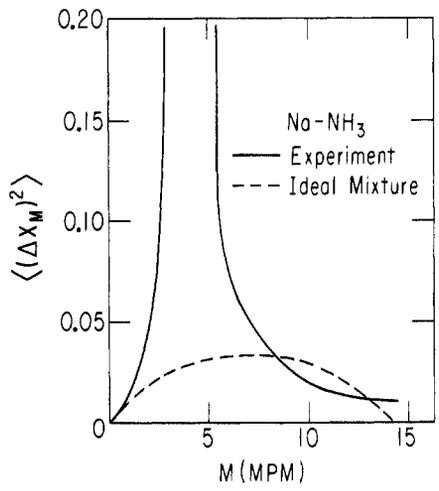

Figure 6. Mean square of concentration fluctuations in Na–HN_3 solutions: solid line, experimental data (ref 83); dashed line, ideal mixture.

$$\langle(\Delta X_M)^2\rangle_{ideal} = X_M[1 - (n+1)X_M] \qquad (V.5)$$

where X_M is the mole fraction of metal. The following features of the data are noteworthy. (1) There are large peaks in the Li and Na data centered about 3.6 MPM for Li and a similar value for Na. (2) These peaks are superimposed on a background similar to what is expected from (V.5). (3) The background differs from (V.5) in two respects, being higher at low concentrations and lower at high concentrations. (4) Cs shows no peak and its value of $\langle(\Delta X_M)^2\rangle$ is similar to the backgrounds for Li and Na for $M < 16$ MPM. (5) $\langle(\Delta X_M)^2\rangle$ for Cs above 20 MPM resembles what is expected from (V.5) for an ideal mixture of $Cs(NH_3)_6$ and Cs.

Regarding the distance scale for concentration fluctuations it was pointed out by Thompson and Lelieur[85] that one can infer from the concentration fluctuation data for Li–NH_3 and Na–NH_3 by a simple argument of Turner[86] the existence of large, high concentration clusters in these materials. Additional evidence for a large distance scale for concentration fluctuations stems from x-ray (X)[87] and neutron (n)[88] small-angle scattering studies. Recent experiments of Chieux[88] on small-angle neutron scattering on 4 MPM Li–ND_3 solutions were analyzed in terms of the Ornstein–Zernike picture of concentration fluctuations. The resulting decay length was $4.7[T_c/(T - T_c)]^{1/2}$ Å at a temperature T above the consolute temperature T_c, which is −58°C for Li–ND_3. This decay length is unusually large,

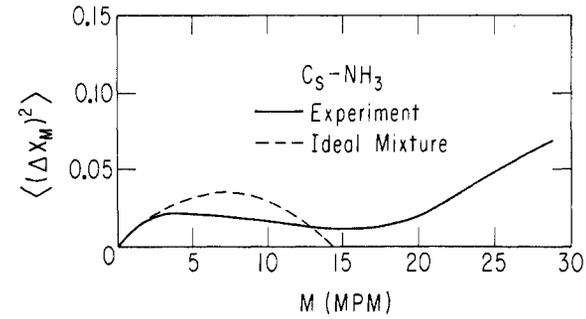

Figure 7. Mean square of concentration fluctuations in Cs–NH_3 solutions: solid line, experimental data (ref 83); dashed line, ideal mixture.

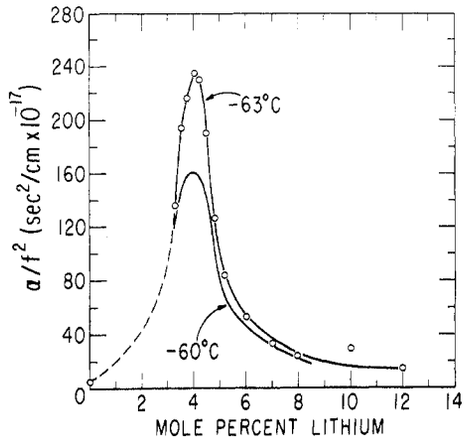

Figure 8. Ultrasonic attenuation in MAS solution after Bowen (ref 89a).

~70 Å at 1 K above T_c and ~10 Å ($>\alpha$) at $T - T_c \simeq 40$ K.

Are these fluctuations distinct from critical fluctuations? Ultrasonic attenuation measurements by Bowen[89] (Figure 8) indicate not only that the fluctuations exist in the 2.3–9 MPM range but that they are distinct from critical fluctuations. The latter are manifested in the ultrasonic attenuation α over a narrow concentration and temperature range about the consolute point as a peak superimposed upon a broad, weakly temperature-dependent maximum. The broad background attenuation we attribute to fluctuations which are, indeed, distinct from critical fluctuations.

Thus, there is strong experimental evidence favoring large amplitude microscopic inhomogeneity at $T - T_c \leq 20$ K on a scale of tens of ångströms in NH_3 solutions of Li and Na, but not of Cs. None of the available experiments proves whether these fluctuations in Li and Na solutions are unimodal or bimodal. Only unimodal concentration fluctuations can occur far away (i.e., when $\zeta \lesssim a$) from T_c, and these are well accounted for in terms of conventional fluctuation theory. Cases of bimodal distribution of local concentration (or density) are, however, also known to occur. The highly developed droplet model of condensation rests on bimodally distributed density fluctuations near the liquid–gas critical point. Many examples of clustering are known both near and unrelated to critical points. Indeed, clustering effects provide the extreme case of a bimodal distribution of concentration fluctuations.

We have proposed for Li and Na solutions at $T - T_c \simeq$ 10–20 K a microscopically inhomogeneous region of the phase diagram of MAS in which (1) the concentration fluctuations are bimodal, varying locally about either of two

well-defined values M_0 and M_1, $M_0 > M_1$; (2) the concentration remains near M_0 or M_1 over radii approximately equal to the short correlation length b for concentration fluctuations; and (3) M_0 is the upper and M_1 the lower bound of the microscopically inhomogeneous region. The concentration fluctuations associated with clusters increase monotonically with cluster size. If the Ornstein–Zernike fluctuation decay length ζ is smaller than b, the concentration would appear to fluctuate abruptly and randomly from M_0 to M_1 or vice versa. We have inferred from Figures 5 and 6 that $M_0 \simeq 9$ MPM and $M_1 \simeq 2.5$ MPM.

Weak experimental evidence for a bimodal distribution of density fluctuations originates from the Thompson–Lelieur analysis[85] of the concentration fluctuation data in terms of the Turner model. Furthermore, the ultrasonic relaxation time[89a] found by Bowen is 5×10^{-8} sec (20 MHz) which is surprisingly long. We propose that it is associated with the time variation of the locally inhomogeneous concentration. Comparable ultrasonic relaxation times (in the range 5–10 MHz) were reported[89b] in aqueous solution of mixed micelles containing two surfactants. There is a close analogy between clustering of solvated electrons and solvated cations in MAS (i.e., bimodal distribution of concentration fluctuations) and micelle formation. These experimental data are indicative but by no means conclusive regarding our proposal of a bimodal distribution of fluctuation.

We now proceed to explore the consequences of the inhomogeneous model regarding electronic structure and transport in MAS.

VI. Allowed Volume Concept

In the microscopically inhomogeneous regime in MAS we propose that the concentration fluctuates locally about either of two well-defined values M_0 and M_1, $M_0 > M_1$, the local concentration remaining near M_0 or M_1 over radii approximately equal to the Debye short correlation length, b, for concentration fluctuations. Provided that b constitutes the largest distance scale parameter involved in the problem, and considerably exceeds λ_F (or l whichever is longer) for the conductive electrons as well as the interionic distance a, the concept of local electronic structure and local response functions can be introduced.[58-62] We then can define an allowed volume fraction $C(E)$ as that fraction of the total volume of the material actually allowed to electrons of energy E. Now, the Weyl theorem[90] tells us that as long as the de Broglie wavelength, or the phase coherence length, is sufficiently small compared to the dimensions of the allowed regions, the density of states will be independent of the geometry of the allowed regions and of the boundary conditions presented by the forbidden regions and proportional to the allowed volume. Thus we may take[58-62,91] as a definition of $C(E)$

$$n(E) = n_0(E)C(E) \tag{VI.1}$$

where $n_0(E)$ is the density of states per unit volume of a metallic region of macroscopic extent and $n(E)$ is the actual density of states of the microscopically inhomogeneous material. Defined in this way $C(E)$ allows properly for penetration into the excluded regions. However, for it to be a useful concept, tunneling across the excluded regions must be quantitatively unimportant for the physical properties. We have demonstrated elsewhere[61,62] that for such large values of the correlation length b as we are concerned with here or for large fluctuations in the potential, tunneling effects are negligible.

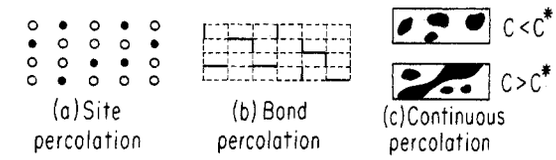

Figure 9. Sketch of different models for classical percolation: (a) site percolation in a two-component system; (b) bond percolation for two types of bonds; (c) continuous percolation for $C < C^*$ and for $C > C^*$.

There are some interesting immediate consequences of this physical picture. The allowed volume concept allows us to establish direct contact with classical percolation theory.[8-13] We are dealing with a continuous site-percolation problem, where any portion of the material can be randomly metallic or nonmetallic. The continuous percolation picture is distinct from the discrete models for site percolation and for bond percolation,[8] as is evident from Figure 9. If $C(E)$ falls below the critical value C^* for classical continuous percolation, percolation theory tells us that a continuous extended path through metallic regions does not exist. The metallic wave functions are therefore localized at that energy. We note in passing that the continuous percolation concept is strictly applicable provided that the conductivity of the nonmetallic regions is vanishingly small. If this is not the case, the concept of a percolation threshold does not strictly apply, but instead we encounter a continuous change of σ, which is finite for all values of C.

The above definition of $C(E)$ should make clear that

$$C(E_F) = C \tag{VI.2}$$

is just the metallic volume fraction, that fraction of the volume of the material in which it is locally metallic. Provided the Fermi level E_F lies close to the middle of the fluctuating semiconducting gaps, the condition for a metal–semiconductor transition in the inhomogeneous transport regime is obtained from eq IV.1 and IV.2

$$C = C(E_F) = n(E_F)/n_0(E_F) = C^* \tag{VI.3}$$

The continuous site-percolation problem has not yet been solved. Existing numerical studies[8] for three-dimensional lattices give values of C^* ranging from $C^* = 0.195$ for fccub to 0.30 for the single crystal. Zallen and Scher[9] suggest that for percolation in a continuous potential $C^* = 0.15$. Skal, Shklovskii, and Efros[12] find $C^* = 0.17$ for the percolation probability in a particular random potential. Webman, Cohen, and Jortner[13] obtained $C^* = 0.15 \pm 0.02$ from numerical simulations of the conductivity of cubic resistor networks with correlated bonds.

We are dealing with an inhomogeneous transport regime in a disordered system, $0 < C < 1$, $C = C(E_F)$. The inhomogeneous regime can be subdivided into two parts. (a) Pseudometallic regime: $1 > C > C^*$. Above the percolation limit the major contribution to transport originates from the continuous extended metallic paths. The transport properties will exhibit a gradual change from those corresponding to the lower limit of the homogeneous metallic regime. (b) Pseudononmetallic regime: $0 < C < C^*$. Here extended states do not exist and tunneling between isolated metallic regions can be ignored.

Finally, we have to establish the relation between the values of C and the mean value

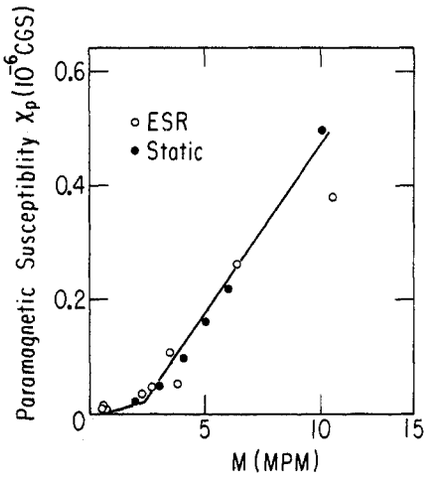

Figure 10. Volume spin susceptibility data for Na–NH_3 solutions (ref 87, 103–106) in the intermediate concentration range. A fit to a two-line-segment function, eq VII.1 and VII.6, is shown.

$$M = \int_0^\infty mP(m)\,dm \qquad \text{(VI.4)}$$

of the mean concentration in MAS. Such a relation we term a C scale. For the special case of a bimodal distribution as we are concerned with here we set approximately

$$P(m) = [(M - M_1)/(M_0 - M_1)]\delta(m - M_0) \times [(M_0 - M)/(M_0 - M_1)]\delta(m - M_1) \qquad \text{(VI.5)}$$

where M_1 and M_0 are the local value of M corresponding to nonmetallic and the metallic regions, respectively. The C scale is

$$C = (M - M_1)/(M_0 - M_1) \qquad \text{(VI.6)}$$

a linear relation between C and M.

We establish the C scale in microscopically inhomogeneous materials in two steps. First, we determine the limits of the inhomogeneous regime from the available structural, thermodynamic, transport, and magnetic data. For a bimodal distribution we take $C = 1$ for $M = M_0$ and $C = 0$ at $M = M_1$. Second, we utilize volume susceptibility data $\chi_p(M)$, when available, to establish the C vs. M relation in the inhomogeneous regime. Because for the materials under consideration local field corrections are negligible in χ_p, the volume spin susceptibility can be written as a superposition

$$\chi_p = C\chi_0 + (1 - C)\chi_1 \qquad \text{(VI.7)}$$

where χ_0 and χ_1 define metallic and nonmetallic susceptibilities at $C = 1$ and at $C = 0$, respectively. Complementary information concerning the C scale originates from Knight shift data.

VII. The C Scale and Analysis of Magnetic Data in MAS

We now establish the relation between the metal concentration M and the metallic volume fraction for metal–ammonia solutions. Regarding the upper limit, $C = 1$, we have already noted that the anomalously large concentration fluctuations[83] disappear into the background at $M \simeq 9$ ppm in the Li and Na solutions, Figures 5 and 6. It is interesting that the Hall constant,[32-35] R, for Li begins to exceed the free electron value R_{fe} for $M < 9$ MPM, and that the conductivity[30,32-35] there becomes of order $10^3\ \Omega^{-1}\ cm^{-1}$ for Li and Na solutions while $k_F l \sim 3$. We recall that for expanded Hg[7] the propagation regime terminates at $k_F l \simeq 2.3$. These three facts together indicate the termination of the homogeneous propagation regime at 9 MPM. Coupling these facts about the transport properties with the evidence for inhomogeneity exposed in section IV leads us to identify the upper limit of the inhomogeneous transport regime as $C = 1$ at 9 MPM in Li and Na solutions. Turning now to the lower limit, $C = 0$, the concentration fluctuations[83] in Li solutions, Figure 5, suggest that the material becomes homogeneous again at $M \simeq 2.5$ MPM. Accordingly, we set $M \simeq 2.5$ MPM as the lowest limit, $C = 0$, of the inhomogeneous regime, and refine this value of M for $C = 0$ to 2.3 MPM by analysis of the magnetic data.

The best available data for the spin susceptibility[39-42,84] are shown in Figure 10. For Na solutions χ_p becomes appreciable above 1 MPM, increasing monotonically with M. It is linear with M in the range $3 < M < 9$ MPM, where it follows

$$\chi_p = \frac{M - 2}{7}\chi_0 \qquad \text{(VII.1)}$$

where $\chi_0 = \chi_p(9)$ is the volume susceptibility in the metallic regions. The bimodal distribution immediately implies that

$$M = 9C + M_1(1 - C) \qquad \text{(VII.2)}$$

which gives us the linear relation

$$C = (M - M_1)/(9 - M_1) \qquad \text{(VII.3)}$$

for the C scale in analogy with eq VI.6. Next, we utilize eq VII.3 for χ_p. Inserting (VII.1) in (VI.7) and defining

$$r = \chi_1/\chi_0 \qquad \text{(VII.4)}$$

where χ_1 is the susceptibility of the nonmetallic regions, yields the relation

$$M_1 = 2 + 7r \qquad \text{(VII.5)}$$

between the two parameters M_1 and r.

Since χ_p is linear in M at least down to 3 MPM and C is linear in M according to (VII.3), (VI.7) plus (VII.5) imply that $2 < M_1 < 3$ MPM. Accordingly we have to introduce a fitting function for χ_p in that range. We have chosen a fit to two linear segments, eq V.12 for $M > 2.33$ MPM and for

$$\chi_p = \frac{M - 1}{28}\chi_0 \qquad \text{(VII.6)}$$

for $M < 2.33$ MPM. Inserting M_1 into (VII.6) give χ_1 and r gives $M_1 = 2.33$. Accordingly we choose our C scale as

$$C = (M - 2.3)/(9 - 2.3) \qquad \text{(VII.7)}$$

and show in Figure 10 the corresponding fit of the χ_p data.

VIII. Response Functions of Microscopically Inhomogeneous Materials

We now address ourselves to the calculation of transport properties of microscopically inhomogeneous materials. We shall refrain from providing detailed derivations and restrict ourselves to quoting mostly new results from our yet unpublished work.

A. Electrical Transport. We now address the problem of calculating the macroscopic transport properties of a material which is locally nonuniform. Consider first the electri-

cal conductivity. In simulating electrical transport properties of a microscopically inhomogeneous material we are dealing with a continuous site-percolation problem in which any portion of the material can be randomly metallic or nonmetallic. To mimic the features of the continuous conduction problem, one can impose correlations on neighboring bonds, so that if a bond is of one type all its neighbors out to the correlation distance b must be of the same type. Together with Webman[13] we have carried out a numerical study of the conductivity of simple cubic resistor networks with correlated bonds. For $x = 0$, the conductivity must vanish for C below the percolation threshold. The major effect of correlations is to shift the percolation threshold from $C^* = 0.25$ for the uncorrelated network[10,11] to $C^* = 0.15 \pm 0.02$, in accord with numerical simulation of the percolation probability[9,12] in the continuous percolation problem. In the particular case of a bimodal distribution of local conductivities, the macroscopic conductivity, σ, was expressed in the form

$$\sigma = \sigma_0 \, \mathrm{f}(x, C) \qquad x = \sigma_1/\sigma_0 \tag{VIII.1}$$

where σ_0 and σ_1 correspond to the conductivities at $C = 1$ and at $C = 0$, respectively. The effective medium theory (EMT) for the conductivity[10,11,58,92-95]

$$\mathrm{f}(x, C) = a + (a^2 + x/2)^{1/2} \qquad a = \frac{1}{2}\left[\left(\frac{3}{2}C - \frac{1}{2}\right)(1 - x) + \frac{x}{2}\right] \qquad x = \sigma_1/\sigma_0 \tag{VIII.2}$$

was found accurate for $0.4 < C < 1.0$ for all values of the conductivity ratio x, in agreement with Kirkpatrick's original work.[10] Serious deviations from the EMT occur for $C < 0.4$ for small values of x (<0.03). This is not surprising, as the EMT, which rests on a mean field approximation for the local conductivity, overestimates the percolation threshold for $x = 0$, $C_{\mathrm{EMT}}^* = \frac{1}{3}$, and can in general be expected to result in too low values of σ for $C < 0.4$ and $0 \leq x < 3 \times 10^{-2}$.

The above theory of the conductivity of an inhomogeneous system is applicable in the inhomogeneous transport regime provided that the phase coherence length for the conduction electrons within the metallic regions is considerably shorter than the correlation length b. When the transport within extended metallic clusters corresponds to the propagation case, as is the case for metal–ammonia solutions, the mean free path is comparable to the sampling length $L = 2b$. In that case, scattering off metallic cluster boundaries reduces the conductivity below the value σ_0 at $C = 1$. The reduction of the metallic conductivity below σ_0 is concentration dependent because the mean cluster size decreases with decreasing concentration. We have accounted for the consequent dependence of the conductivity of the metallic region on C by a modification of Eggarter's theory for scattering from the boundaries of the allowed regions.[96] The two conductivities are related by

$$\sigma_0(C)/\sigma_0 = \lambda(C)/l \tag{VIII.3}$$

where l is the mean free path at $C = 1$, while $\lambda(C)$ is the mean free path in the allowed volume fraction C. The latter quantity is given by Eggarter in the form[96]

$$\lambda(C) = l\lambda_s/(l + \lambda_s) \tag{VIII.4}$$

where in our case the mean free path λ_s associated with scattering by prohibited regions at the boundaries of the allowed regions is

$$\lambda_s = \sum_{n=1}^{\infty} 2nbC^{n-1}(1 - C) = 2b[1 - C]^{-1} \tag{VIII.5}$$

Thus from eq VIII.3–VIII.6 we obtain

$$D(C) = \frac{\sigma_0(C)}{\sigma_0} = \frac{z}{1 - C + z} \tag{VIII.6}$$

where

$$z = 2b/l \tag{VIII.7}$$

We impose no corresponding correction to σ_1 from scattering from the boundaries of the nonmetallic regions. We should note in passing that when the metallic region corresponds to the diffusion limit $z \geq 2b/a$ holds, where a is the interatomic spacing, so that $z \gg 1$ and $D(C) \to 1$ for all C.

The classical expression for the conductivity, eq VIII.2, has now to be modified by accounting for the dependence of $\sigma_0(C)$ on the fraction of allowed volume so that

$$\sigma = \bar{\mathrm{f}} D(C)\sigma_0 \tag{VIII.8}$$

where

$$\bar{\mathrm{f}} = \mathrm{f}[C, x(C)] \tag{VIII.9}$$

$$x(C) = \frac{\sigma_1}{\sigma_0 D(C)} = \frac{x}{D(C)} \tag{VIII.10}$$

and now $x(C)$, eq VIII.10 replaces x in eq VIII.2. Equations VIII.8–VIII.10 constitute a modified effective medium theory (EMTZ). For materials characterized by $x > 3 \times 10^{-2}$ the EMTZ is applicable throughout the entire range $0 < C < 1$. For materials where $x < 3 \times 10^{-2}$ the EMTZ is valid only for $0.5 < C < 1.0$, while for $C < 0.5$ we have utilized eq VIII.1 where $\bar{\mathrm{f}}$, eq VIII.9, can be obtained from numerical simulations of σ/σ_0 in a correlated cubic network, with $x(C)$ given by eq VIII.10.

We were unable to go beyond the EMT for the galvanomagnetic properties of inhomogeneous materials. The EMT yields[97] for the Hall coefficient, R, and for the Hall mobility, μ

$$\mu/\mu_0 = \mathrm{g}(x, y, \mathrm{f}) = [1 - B(1 - xy)]\mathrm{f}^{-1} \tag{VIII.11}$$

$$R/R_0 = \mathrm{h}(x, y, \mathrm{f}) = [1 - B(1 - xy)]\mathrm{f}^{-2} \tag{VIII.12}$$

$$B = \frac{(2\mathrm{f} + 1)^2(1 - C)}{(2\mathrm{f} + 1)^2(1 - C) + (2\mathrm{f} + x)^2 C} \qquad y = \mu_1/\mu_0 \tag{VIII.13}$$

where μ_0 and μ_1 are the Hall mobilities in the metallic and in the semiconducting regions, corresponding to the Hall mobilities at $C = 1$ and at $C = 0$, respectively. When boundary scattering effects are incorporated EMTZ yields correspondingly

$$R = \bar{\mathrm{h}} R_0 \tag{VIII.14}$$

$$\mu = \bar{\mathrm{g}} D(C)\mu_0 \tag{VIII.15}$$

$$\bar{\mathrm{g}} = \mathrm{g}[C, x(C), y(C), \bar{\mathrm{f}}] \tag{VIII.16}$$

$$\bar{\mathrm{h}} = \bar{\mathrm{g}}/\bar{\mathrm{f}} \qquad x(C) = x/D(C) \qquad y(C) = y/D(C) \tag{VIII.17}$$

On the basis of numerical simulations of σ we have concluded that the EMT or the EMTZ hold in general for $C >$

0.4, while for $0 < C < 0.4$ the mean field approximation is adequate for materials where $x > 3 \times 10^{-2}$. We infer that the same will apply for R and μ. On the other hand, for materials where $x < 3 \times 10^{-2}$ for $C < 0.4$ the EMT and the EMTZ provide only a qualitative interpolation formula.

B. Thermal Transport. It is straightforward to carry out an effective medium theory for any tensorial response function, e.g., thermal transport coefficients, optical constants, diffusion coefficients, etc. Such an EMT analysis can be readily generalized into an accurate numerical calculation of a random continuum property for a diagonal response function by the method we have used for the electrical conductivity.

We have carried out an EMT for a system simultaneously subjected to gradients of temperature and electric potential, obtaining explicit expressions for the thermal transport properties of an inhomogeneous material.[58] We start with the microscopic equations

$$\begin{aligned} \vec{J}' &= k'\vec{\nabla}T' + P'T'\vec{\nabla}\varphi' \\ \vec{j}' &= \sigma'\vec{\nabla}\varphi' + P'\vec{\nabla}T' \end{aligned} \qquad \text{(VIII.18)}$$

which holds locally within the inhomogeneous material. Primed quantities indicate local values. J' and j' are the heat and electrical currents, respectively, k' and σ' are thermal and electrical conductivity, respectively. P' is the Peltier coefficient, while φ' and T' are the electrical potential and the temperature, respectively. The corresponding macroscopic equations are identical with (VIII.18) but with unprimed quantities. The relation between the macroscopic and microscopic fluxes and forces is

$$\begin{aligned} \vec{J} &= \langle \vec{J}' \rangle;\ T = \langle T' \rangle \\ \vec{j} &= \langle \vec{j}' \rangle;\ \varphi = \langle \varphi' \rangle \end{aligned} \qquad \text{(VIII.19)}$$

where the average can be taken equivalently over all space or over all local configurations at a given point.

To carry out an effective medium theory of the relation between the macroscopic transport coefficients κ, σ, and P and the corresponding microscopic quantities, we treat the system as though it consisted of a sphere of radius b embedded within a uniform effective medium characterized by the coefficients κ, σ, and P. We use the conservation conditions and Maxwell's equations together with eq VIII.18 to determine J', j', T', and φ' inside the inclusion. Application of eq VIII.19 results in a consistency condition, the EMT condition, which must be satisfied by κ, σ, and P, determining them implicitly in terms of averages over κ', σ', and P'. The result for σ is the usual EMT result, eq VIII.2, that for κ is

$$\left\langle \frac{\kappa - \kappa'}{\kappa' + 2\kappa} \right\rangle = 0 \qquad \text{(VII.20)}$$

while for P we get

$$P = \frac{3\kappa\sigma\langle P'/(\kappa' + 2\kappa)(\sigma' + 2\sigma)\rangle}{\langle(\kappa\sigma' + \sigma\kappa' + 2\kappa\sigma - \kappa'\sigma')/(\kappa' + 2\kappa)(\sigma' + 2\sigma)\rangle} \qquad \text{(VIII.21)}$$

The thermoelectric power, S, can be obtained from eq VIII.21 by substituting

$$S = P/\sigma \qquad \text{(VIII.22)}$$

for primed and unprimed quantities in (VIII.21).

The measured thermal conductivity $\bar{\kappa}$ is given by

$$\bar{\kappa} = \kappa - S^2\sigma T \qquad \text{(VIII.23)}$$

For MAS the second term on the right-hand side of eq VIII.23 is of order $10^{-3}\bar{\kappa}$ and can be neglected.

C. Optical Properties. Finally, we consider the optical properties of microscopically inhomogeneous materials. Together with Webman we have developed[99] an effective-medium theory for the frequency dependent dielectric constant

$$\epsilon(\omega) = \epsilon_1(\omega) + i\epsilon_2(\omega) \qquad \text{(VIII.24)}$$

The EMT condition for $\epsilon(\omega)$ is

$$\left\langle \frac{\epsilon(\omega) - \epsilon^i(\omega)}{2\epsilon(\omega) + \epsilon^i(\omega)} \right\rangle = 0 \qquad \text{(VIII.25)}$$

where $\epsilon^i(\omega)$ is a possible value of the local complex dielectric function and the average is over all such values. For a bimodal distribution of fluctuations $\epsilon^i(\omega)$ takes on a functional form $\epsilon^0(\omega) = \epsilon_1{}^0(\omega) + i\epsilon_2{}^0(\omega)$ characteristic of metallic regions with probability C or $\epsilon^1(\omega) = \epsilon_1{}^1(\omega) + i\epsilon_2{}^1(\omega)$ characteristic of the nonmetallic regions, with a probability $1 - C$. Equation VIII.25 may then be readily solved:

$$\epsilon(\omega) = \epsilon^0(\omega)\, f(C, x(\omega)) \qquad \text{(VIII.26)}$$

$$f(C, x(\omega)) = a(\omega) \pm \left[(a(\omega))^2 + \frac{1}{2}\, x(\omega)\right]^{1/2} \qquad \text{(VIII.27)}$$

$$a(\omega) = \frac{1}{2}\left[\left(\frac{3}{2}\, C - \frac{1}{2}\right)(1 - x(\omega)) + \frac{x(\omega)}{2}\right] \qquad \text{(VIII.28)}$$

$$x(\omega) = \epsilon^1(\omega)/\epsilon^0(\omega) \qquad \text{(VIII.29)}$$

The sign in (VIII.27) is chosen to give positive $\epsilon_2(\omega) = |m|[\epsilon(\omega)]$. Equations VIII.26–VIII.29 represent a generalization of the EMT for a real, diagonal, second-order tensor to the complex case. Our experience with the former case leads us to expect that the EMT is accurate for all values of C if $|x(\omega)|$ is within the range 0.03–30. Numerical simulations[99] of $\epsilon(\omega)$ in a simple cubic network bear out this expectation.

D. Sound Velocity. We have recently extended the effective-medium theory to the case of wave propagation in a microscopically inhomogeneous medium[100] in which the propagation velocity takes a random value c_i which remains constant over a correlation radius b. The familiar effective-medium condition

$$\left\langle \frac{c_i{}^2 - \bar{c}^2}{c_i{}^2 + 2\bar{c}^2} \right\rangle = 0 \qquad \text{(VIII.30)}$$

results for the macroscopic propagation velocity $\bar{c}$, where the average is taken over all values of local velocity c_i. For a bimodal distribution of fluctuations c_i takes the values c_0 with probability C or c_i with probability $1 - C$, whereupon (VIII.30) results in

$$\begin{aligned} \bar{c}^2 &= c_0{}^2 f(X_s, C) \\ X_s &= c_1{}^2/c_0{}^2 \end{aligned} \qquad \text{(VIII.31)}$$

and the function $f(X_s, C)$ is defined in terms of eq VIII.2.

IX. Analysis of Response Functions for MAS

We now proceed to the analysis of the transport properties of disordered materials undergoing a metal–nonmetal transition via the inhomogeneous transport regime. In section V we have established the limits of the inhomogeneous transport regime and the C scale. The parameters needed as input data for the analysis of the transport properties are the transport coefficients at $C = 1$ and at $C = 0$. These are taken from experiments and listed in Table II.

TABLE II: Values of the Ratios of Electronic and Thermal Transport Coefficients Associated with the Limits of the Inhomogeneous Regime in MAS

	$C = 0$	$C = 1$	x	y	κ_1/κ_0	S_1/S_0	c_S^1/c_S^0	Sources of experimental data
Li–NH_3 (223 K)	M = 2.3 MPM	M = 9 MPM	1.2×10^{-3}	8×10^{-3}			1.33	2–5, 26–38, 43, 44
Na–NH_3 (240 K)	M = 2.3 MPM	M = 9 MPM	2.4×10^{-3}		0.35	20	1.33	101, 102

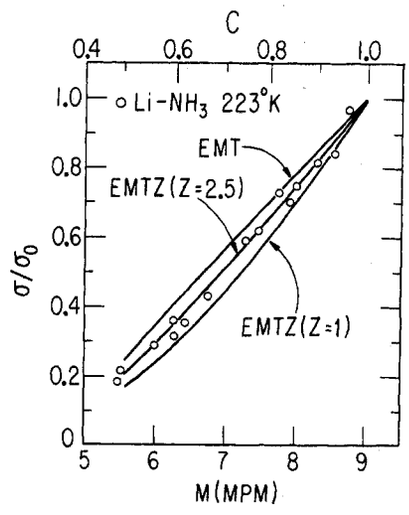

Figure 11. Analysis of the electrical conductivity data of Li–NH_3 solutions, 5.5 MPM < M < 9 MPM, at T = 223 K (ref 30–37), in terms of the modified effective medium theory (EMTZ). The best fit is obtained for z = 2.5. The curves for $z = \infty$ (EMT) and for z = 1 are shown for comparison.

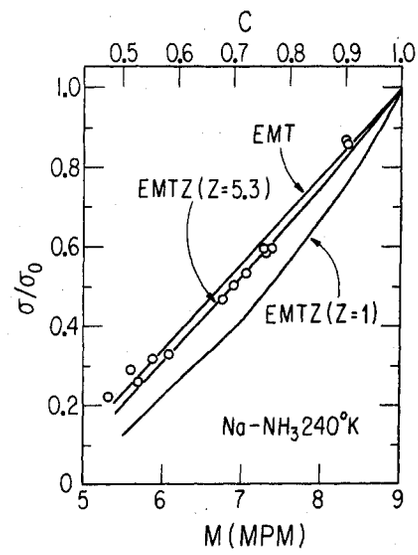

Figure 12. Analysis of the electrical conductivity data of Na–NH_3, 5.5 MPM < M < 9 MPM, at T = 240 K (ref 28 and 29), in terms of the EMTZ. The best fit is obtained for $z = 5.3 \pm 0.6$. Also shown are the curves for $z = \infty$ and z = 1.

For small x and y, i.e., $x \sim 10^{-3}$ to 10^{-4} and $y \sim 10^{-2}$ to 10^{-3}, as is appropriate to metal–ammonia solutions, the transport coefficients in the range $4 < C < 1.0$ are independent of x and y. Thus the EMT equations (VIII.2) or the EMTZ relations (VIII.8–VIII.10) apply for $C > 0.4$. Both σ and μ drop rapidly while R varies slowly in this range of C. The conductivity assumes the simple form

$$\sigma = \sigma_0 \left(\frac{3}{2}C - \frac{1}{2}\right) \qquad 0.4 < C < 1.0 \qquad \text{(IX.1)}$$

while the galvanomagnetic transport coefficients are

$$R = 4R_0/(3C + 1) \qquad \text{(IX.2)}$$

$$\mu = \mu_0 \left(\frac{6C - 2}{3C + 1}\right) \qquad \text{(IX.3)}$$

When boundary scattering corrections are required they do not affect the value of R, eq VIII.14, while σ and μ are modified to

$$\sigma = \sigma_0 D(C) \left(\frac{3}{2}C - \frac{1}{2}\right) \qquad \text{(IX.4)}$$

$$\mu = \mu_0 D(C) \left(\frac{6C - 2}{3C + 1}\right) \qquad \text{(IX.5)}$$

in this range of C. For lower values of C (<0.4) we assert on the basis of numerical simulations that σ continues to decrease. We expect the Hall mobility to exhibit a similar decrease in the range $0 < C < 0.4$.

We now proceed to the analysis of the conductivity data. We have compared σ/σ_0 with eq IX.1 for Li and Na for 9 MPM > M > 5.5 MPM and show the results in Figures 11 and 12. The data fall systematically below the EMT, more so for Li than for Na. We therefore fitted the data to the EMTZ, adjusting the one parameter z to get a best fit. The results are also shown in Figures 11 and 12 for the best fit with z = 2.5 for Li while at least-squares analysis results in $z = 5.3 \pm 0.6$ for Na. Also shown is EMTZ for z = 1 for comparison. From these values of z a rough estimate of b can be obtained. Using the weak scattering, nearly free electron form for σ_0, we estimate the mean free path to be 12 Å for Li and Na. The corresponding values of b from eq VIII.8 are

$$\begin{aligned} b &= 15 \text{ Å} \quad \text{Li–NH}_3,\ T = 223 \text{ K} \\ b &= 32 \text{ Å} \quad \text{Na–NH}_3,\ T = 240 \text{ K} \end{aligned} \qquad \text{(IX.6)}$$

The fit to the EMT breaks down seriously at low concentration, and the EMTZ is little different there. Accordingly, we have compared the experimental data with various numerical simulations in Figures 13 and 14 for Li and for Na. One sees that as the range of correlation is increased so that continuum percolation is approached, the fit becomes excellent over three orders of magnitude of variation in σ. It should be recognized that the theoretical curve is fixed to the experimental data at the C = 0 and C = 1 end points of the inhomogeneous range but that otherwise there are no adjustable parameters. (We have ignored the EMTZ corrections in the present context.) The simulations should be regarded, therefore, as interpolations between the end points and they serve excellently as such. There should be little doubt now as to the existence of an inhomogeneous transport regime for 2.3 MPM < M < 9 MPM.

Next, we consider the Hall data for this system. Since we have been unable to go beyond the EMT for the galvanomagnetic properties, we have compared the available Li Hall data[32–35] to the effective medium theory. As we have already noted, in this material the boundary scattering cor-

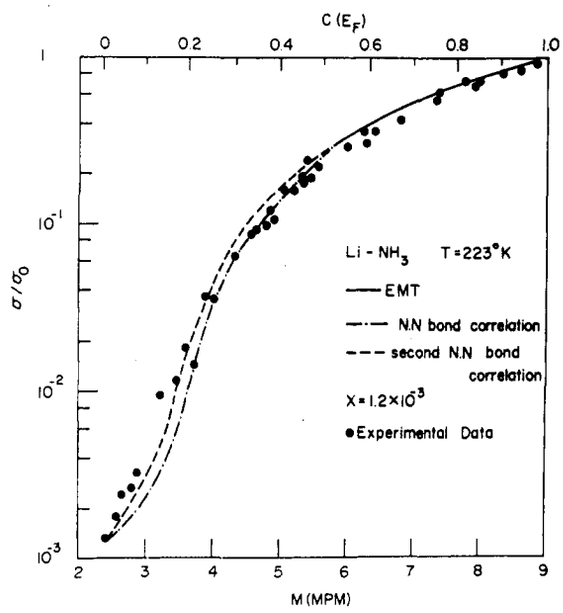

Figure 13. Analysis of the electrical conductivity data of Li–NH_3 solutions at 223 K (ref 32–37) throughout the entire inhomogeneous regime $C = 1$ at 9 MPM and $C = 0$ at 2.33 MPM: solid curve ($C > 0.5$), EMT; dotted-dashed curve, numerical simulation with nearest neighbor bond correlation ($x = 1.2 \times 10^{-3}$); dashed curve, numerical simulation with second nearest neighbor bond correlation ($x = 1.2 \times 10^{-3}$). Circles represent experimental data.

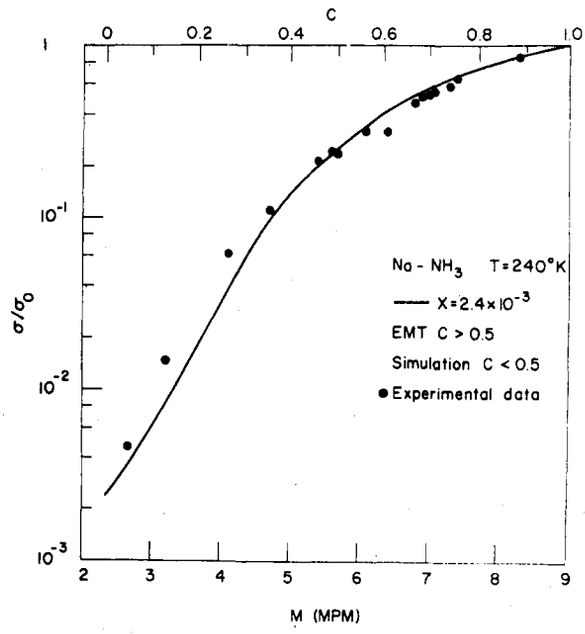

Figure 14. Analysis of the electrical conductivity data of Na–NH_3 solutions at 240 K (ref 28 and 29) throughout the entire inhomogeneous regime $C = 1$ at 9 MPM and $C = 0$ at 2.33 MPM: solid curve, EMT for $C > 0.5$ and numerical simulations with second nearest neighbor bond correlation ($x = 2.4$ and 10^{-3}) for $C < 0.5$. Circles represent experimental results.

rections to R are negligible for $C > 0.4$, while in the low C range ($0 < C < 0.4$) the EMT is inaccurate and there is little point to introduce the modified EMTZ version of the theory. In Figure 15 we portray the available Li Hall effect data together with the EMT curve using the experimental data at $C = 0$ and $C = 1$ from Table II. In the pseudometallic regime down to $C = 0.4$ the agreement between theory

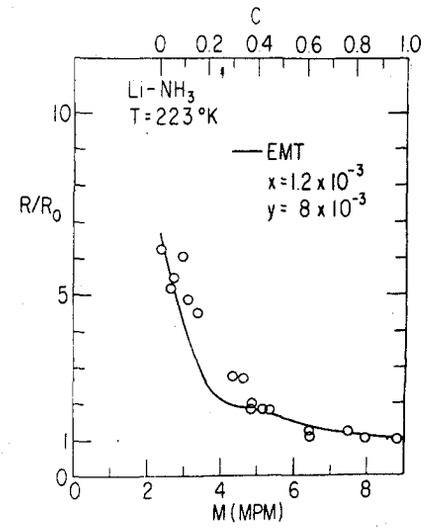

Figure 15. Analysis of Hall effect data (ref 33 and 34) of Li–NH_3 solutions at 223 K in terms of the EMT.

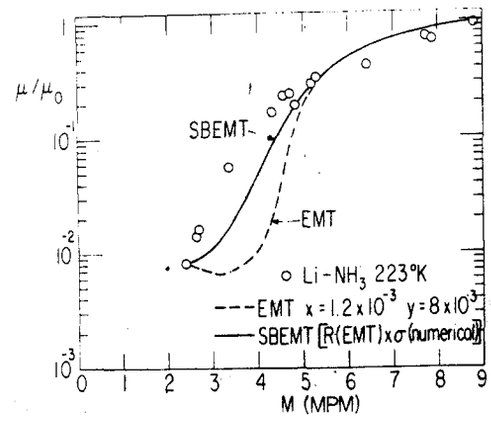

Figure 16. Analysis of the Hall mobility data (ref 33 and 34) for Li–NH_3 solutions at 223 K in terms of the effective-medium theory (dashed line) and the SBEMT (solid line).

and experiment is good, while for $0 < C < 0.4$ the EMT curve provides just an approximate interpolation formula.

In view of the quantitative agreement of σ and the reasonable agreement of R with the predictions of the EMT (and EMTZ) in the range $0.4 < C < 1$ it is apparent that a good fit can be obtained for the concentration dependence of the Hall mobility, μ, in this range as is evident from Figure 16. The small negative deviations of μ from the EMT curve in the concentration range 5 MPM $< M <$ 9 MPM can be readily accounted for in terms of boundary scattering effects; however, the experimental Hall mobility data are not accurate enough to warrant a detailed analysis in terms of the EMTZ. In the lower concentration range $C <$ 0.4 the experimental data exhibit a marked deviation from the EMT curve. This is not surprising as the EMT for σ reveals deviations in that range. In the absence of a numerical simulation scheme for R and μ, we have compromised by taking for μ the product of R obtained from EMT and μ as derived from the numerical simulation. The resulting curve, labeled as SBEMT in Figure 16, substantially improves the agreement with experiment.

We now turn to the analysis of the thermal conductivity[43] and the thermoelectric power[44,45] for Li and Na solutions. The available thermal conductivity data for Na–NH_3

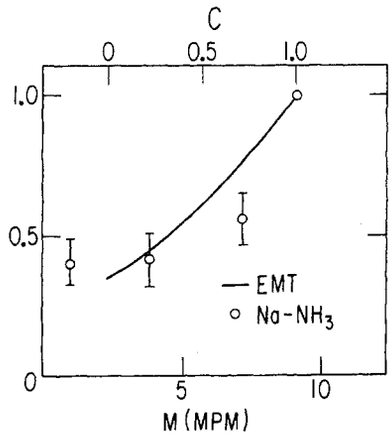

Figure 17. Analysis of the available thermal conductivity data (ref 43) for Na–NH_3 solutions in terms of the EMT.

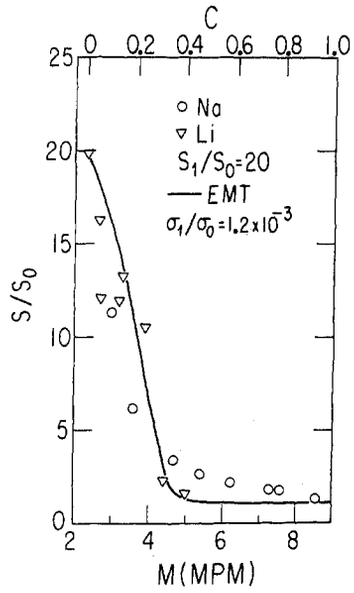

Figure 18. Analysis of the thermoelectric power data (ref 44 and 45) for Na–NH_3 and for Li–NH_3 solutions. The solid EMT curve is drawn for $S_1/S_0 = 20$, $\kappa_1/\kappa_0 = 0.35$, and $\sigma_1/\sigma_0 = 1.2 \times 10^{-3}$. Increasing x by a factor of 2 has small (~1%) effect in the range $C < 0.4$ where the EMT is inaccurate.

can be fitted by the EMT equation with $\kappa_1/\kappa_0 = 0.35$–0.40. The available experimental data,[43] Figure 17, are too sparse and inaccurate to attempt a quantitative correction for boundary scattering. Finally, it is worthwhile to note that for this system the high κ_1/κ_0 ratio implies that the EMT for the thermal conductivity is valid throughout the whole C range.

The thermoelectric power data for Li and Na solutions,[44,45] Figure 18, are in reasonable agreement with the EMT curve calculated from eq VIII.21 and VIII.22 with the parameters shown in Table II. We note in passing that as the general EMT expression, eq VIII.21 and VIII.22 for S, involves the local conductivity σ_1, which exhibits a large fluctuation for this system, we do not expect the EMT for S to be accurate as for κ for $C < 0.4$. It is important to note that the very weak variation of S with C in the range $0.4 < C < 1$ predicted by EMT and found in the data is a feature of the bimodal distribution of M values. A unimodal distribution would give a more nearly linear interpolation between $C = 0$ and $C = 1$.

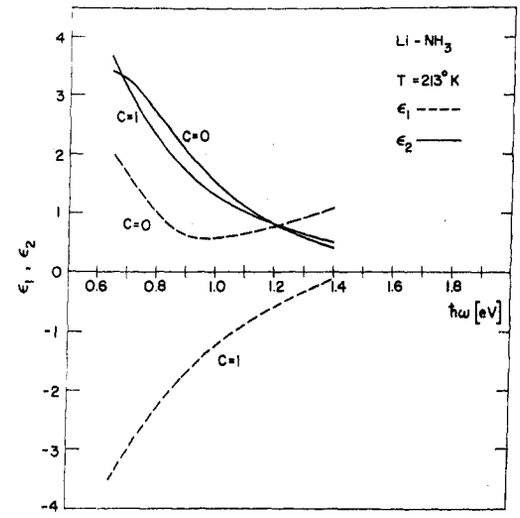

Figure 19. $\epsilon^0(\omega)$ and $\epsilon^1(\omega)$ for Li–NH_3 solutions at 213 K.

We now turn to the optical data of MAS. At concentrations above 8 MPM $\epsilon_1(\omega)$ and $\epsilon_2(\omega)$ differ for Li–NH_3 and Na–NH_3 solutions only in details from the behavior expected for a Drude, free-electron system. In the concentration range 8–2 MPM, which corresponds approximately to the inhomogeneous regime, $\epsilon_1(\omega)$ exhibits a continuous variation from metallic toward a behavior characteristic of a very broad resonance at ~0.6 eV. This is consistent with the behavior of $\epsilon_2(\omega)$, which is Drude-like and shows a slow variation with M in the range 4–8 MPM, with an indication of a resonance around 0.6 eV at 2–3 MPM. Thompson and colleagues[47,48] point out that there are signs of persistence of the bound-electron absorption to quite high concentrations, 6 MPM. This mixed behavior of optical properties is consistent with our model for microscopic inhomogeneities in these solutions in that concentration range and lends further point to our attempts to account for the optical data in terms of our theory. As in these systems $|x(\omega)|$, eq VIII.28, is in the range 0.1–10 the condition for the applicability of the EMT, eq VIII.26–VIII.29 are well met. We now turn to the analysis of Li–NH_3 optical data at 213 K in terms of the EMT. We choose a Drude–Lorentz form for $\epsilon^0(\omega)$

$$\epsilon^0(\omega) = \epsilon_\infty - \frac{\omega_p^2}{\omega(\omega + i/\tau)} \qquad \text{(IX.7)}$$

with the parameters $\epsilon_\infty = 1.35$, $\hbar\omega_p = 1.8$ eV, and $\hbar/\tau = 0.5$ eV. $\epsilon^1(\omega)$ at 2.3 MPM ($C = 0$) is not available, and we had to follow an indirect route in evaluating $\epsilon^1(\omega)$. $\epsilon^1(\omega)$ was determined by inserting (IX.7) and the experimental values of $\epsilon(\omega)$ into (VIII.26)–(VIII.29) for $M = 3$ MPM (i.e., $C = 0.1$) and solving for $\epsilon^1(\omega)$. The results for $\epsilon^0(\omega)$ and $\epsilon^1(\omega)$ are shown in Figure 19. Next, calculations for $\epsilon(\omega)$ were made for $M = 4$ MPM ($C = 0.25$), $M = 5$ MPM ($C = 0.4$), and $M = 8$ MPM ($C = 0.85$). The comparison between theory and experiment (Figures 20 and 21) is as good as can be expected. We therefore believe that bound-electron absorption persists well into the intermediate range and that this persistence is a strong evidence for compositional inhomogeneities in this composition range.

Finally, we consider the sound velocity data for Bowen et al.[101,102] The sound velocity c_0 at 9 MPM is taken as 1678 m sec^{-1} for Li–NH_3 at 223 K and 1376.2 m sec^{-1} for Na–NH_3 at 240 K, while for c_1 we take 1678 m sec^{-1} for Li–

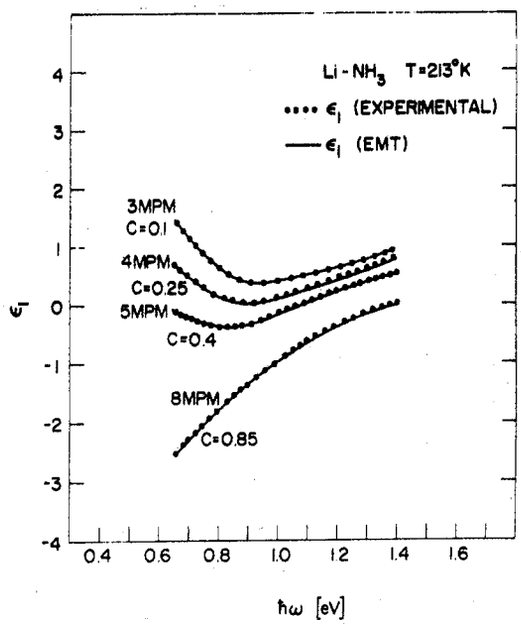

Figure 20. Concentration dependence of $\epsilon_1(\omega)$ of Li–NH_3 solutions at 213 K. Points represent experimental data (ref 47 and 48).

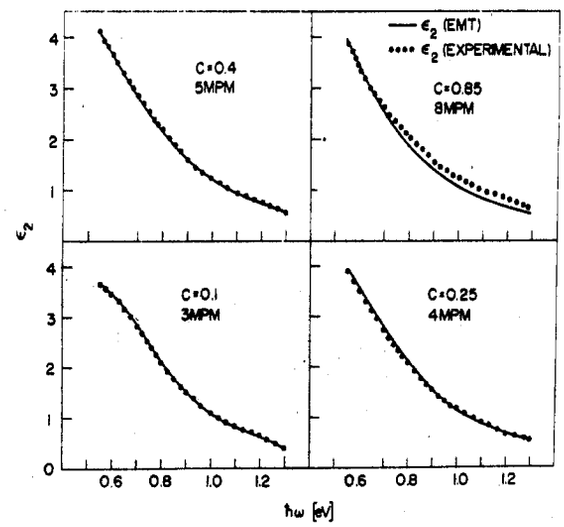

Figure 21. Concentration dependence of $\epsilon_2(\omega)$ for Li–NH_3 solutions at 213 K. Points represent experimental data (ref 47 and 48).

NH_3 at 223 K and 1608.4 m sec^{-1} for Na–NH_3 at 240 K. The fit to the EMT, eq VIII.31, is shown in Figure 22. It should, however, be pointed out that for a value of X_s, 1.32, as large as occurs here, the agreement between theory and experiment for the sound velocity data provides no further confirmation of our model for MAS.

X. Concluding Remarks

We have built up strong evidence for continuous MNMT intermediated by microscopic inhomogeneities in the two component systems Li and Na ammonia solutions at $|T - T_c| \simeq$ 10–20 K. These materials were selected for detailed study because of the availability of extensive experimental data. Our theory provides the first semiquantitative approach for the understanding of the variation of the response functions in a class of disordered materials which undergo a "continuous" MNMT. Concerning the details of the analysis of response functions of inhomogeneous materials we stress that the analysis of transport and optical data in terms of numerical simulations and the EMT does not involve a curve-fitting procedure. Instead, we connect the transport and optical properties to magnetic data, which are used to derive the C scale. Comparison with observations leads to a good fit between theory and experiment for electrical and thermal transport properties, optical data, and sound velocity data and to the determination of the short correlation length from the analysis of the conductivity data.

The validity of our physical picture has been challenged by Mott.[57] All of the published objections to our approach are explicitly or implicitly refuted.[60-62] We note also that the continuous metal–nonmetal transitions considered by us do not involve a Mott transition, as the electrons are confined either to metallic regions or nonmetallic regions. The ideas advanced by Mott regarding the Hubbard bands in a monovalent metal and the band overlap in a divalent metal have to be applied *locally*.

The basic physical idea advanced by us concerning the MNMT in MAS is that microscopic inhomogeneities determine electronic structure and transport properties within the transition region. We have proposed that for Li–NH_3 and Na–NH_3 in the low temperature range ($T - T_c \lesssim$ 20K) bimodal concentration fluctuations prevail, constituting essentially a physical situation where clustering of solvated electrons and cations occurs. The following transport data are consistent with the assumption of bimodality. First, our analysis of the electrical conductivity which varies over a range of three orders of magnitude would fail if a unimodal distribution were to prevail. Second, the thermoelectric power calculated for the bimodal distribution (Figure 18) exhibits a weak dependence on C for $0.5 < C < 1$, which is also the trend observed in the experimental data. A unimodal distribution would result in a faster increase of S with decreasing M in that region. Finally, the excellent fit of the optical data over a broad energy range supports the bimodality hypothesis. Nevertheless, in our opinion the question of whether the fluctuations in Li– and Na–NH_3 at

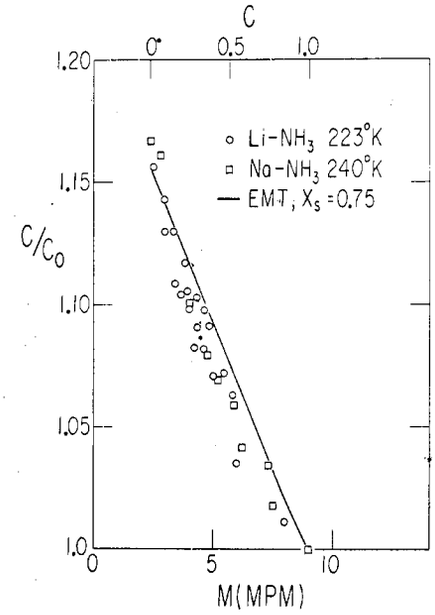

Figure 22. Concentration dependence of the sound velocity data (Bowen, ref 101 and 102) in Li–NH_3 and Na–NH_3.

low $T - T_c$ are unimodally or bimodally distributed remains open, providing a challenging theoretical and experimental problem.

At higher temperatures for Li and Na solutions as well as for Cs solutions over the entire temperature range a normal, unimodal distribution of density fluctuations will intermediate the MNMT. The physical situation is analogous to the case of the MNMT in expanded liquid Hg, briefly considered in section III.

The lower limit of the inhomogeneous regime in Li–NH_3 and Na–NH_3 at 2.3 MPM requires a reinterpretation of the transport properties in the range between ~1 and 2.3 MPM, which we have already considered in section IV. We propose that a pseudointrinsic semiconductivity mechanism prevails. The valence and the conduction bands correspond to σ_g and σ_u orbitals of electron cavity pairs, respectively. In view of the low (~0.6–0.7 eV) σ_g–σ_u separation within a single cavity pair reduction of the band gap due to the broadening of the valence and conduction bands will occur at much lower number density than in expanded semiconducting Hg below 7.8 g cm^{-3}. In the intrinsic semiconducting regime in MAS the major contribution to the conductivity and the paramagnetic susceptibility will result from electrons excited near the mobility edge E_c. Thus χ_p is proportional to the conductivity. We expect that in the concentration range 1–2.3 MPM, $\chi_p = \bar{A}\sigma J^{-2}$, where $\bar{A}$ is a constant and J is the transfer integral in Friedman's theory.[70] The sparse experimental data available are not yet sufficient to test this hypothesis. Regarding the galvanomagnetic properties in that concentration range we expect that according to the Friedman relations[70] for a disordered semiconductor $\mu \propto Jn(E_c)$ so that the Hall mobility will decrease with decreasing M due to the reduction of the transfer integral J.

From the foregoing discussion a coherent picture emerges for the electrical transport properties and the MNMT of MAS in the intermediate concentration range 1–9 MPM. We predict that the Hall coefficient for MAS will decrease throughout the entire concentration range 9–1 MPM which spans the inhomogeneous regime and the semiconducting regime. Furthermore, the microwave properties of MAS would provide extremely useful information on the state of these systems in the transition region. We have treated the microwave dielectric constant by numerical simulations. The results are sensitive to the difference between unimodal and bimodal distributions of density fluctuations. Uncertainty in the available experimental data[103] prevents a comparison with theory. Detailed experimental evidence on the microwave properties of MAS will be of considerable importance.

Acknowledgments. We are indebted to I. Webman for his help with the numerical analysis, to S. Kirkpatrick for providing us with his computer program, to J. C. Thompson and to D. A. Bowen for supplying detailed experimental results, and to N. R. Kestner, J. C. Thompson, and I. Webman for helpful discussions.

References and Notes

(1) Based on research supported by the ARO(D), the L. Block Fund, and the Materials Research Laboratory of the National Science Foundation at The University of Chicago, and by the U.S.-Israel Binational Science Foundation at the University of Tel-Aviv.
(2) (a) "Metal Ammonia Solutions", G. Lepoutre and M. J. Sienko, Ed., W. A. Benjamin, New York, N.Y., 1964; (b) "Metal Ammonia Solutions", J. J. Lagowski and M. J. Sienko, Ed., Butterworths, London, 1970.
(3) "Electrons in Fluids", Proceedings of Colloque Weyl III on Metal-Ammonia Solutions, J. Jortner and N. R. Kestner, Ed., Springer-Verlag, Heidelberg, 1973, p 257.
(4) M. H. Cohen and J. C. Thompson, *Adv. Phys.*, **17**, 857 (1968).
(5) R. Catteral and N. F. Mott, *Adv. Phys.*, **18**, 665 (1969).
(6) N. F. Mott, "Metal-Insulator Transitions", Taylor and Francis, London, 1974.
(7) H. Endo, A. I. Eatah, J. G. Wright, and N. Cusack, *J. Phys. Soc. Jpn.*, **34**, 666 (1973).
(8) V. K. S. Shante and S. Kirkpatrick, *Adv. Phys.*, **20**, 325 (1971).
(9) R. Zallen and H. Scher, *Phys. Rev., B*, **4**, 4471 (1971).
(10) S. Kirkpatrick, *Phys. Rev. Lett.*, **27**, 1722 (1971).
(11) S. Kirkpatrick, *Rev. Mod. Phys.*, **45**, 574 (1973).
(12) A. S. Skall, B. I. Shlovskil, and A. L. Efros, *JETP Lett.*, **17**, 522 (1973).
(13) I. Webman, J. Jortner, and Morrel H. Cohen, *Phys. Rev. B*, **11**, 2885 (1975).
(14) F. Hensel and E. U. Franck, *Ber. Bunsenges. Phys. Chem.*, **70**, 1154 (1966).
(15) R. Schmutzler, F. Hensel, and E. U. Franck, *Ber. Bunsenges. Phys. Chem.*, **72**, 1194 (1968).
(16) E. U. Franck and F. Hensel, *Phys. Rev.*, **147**, 109 (1967).
(17) R. W. Schmutzler and F. Hensel, *Ber. Bunsenges. Phys. Chem.*, **76**, 347 (1972).
(18) F. Hensel and R. W. Schmutzler, *J. Non-Cryst. Solids*, **8–10**, 718 (1972).
(19) F. Hensel, *Phys. Lett.*, **31**, 88 (1970).
(20) U. Even and J. Jortner, *Phys. Rev. Lett.*, **28**, 31 (1972); *Phys. Rev. B*, **8**, 2536 (1973).
(21) U. Even and J. Jortner, *Phil. Mag.*, **25**, 715 (1972).
(22) M. Zillgit, Thesis, Karlsruhe University, Germany, 1972.
(23) M. Zillgit and F. Hensel, submitted for publication.
(24) U. Even and J. Jortner, *Phil. Mag.*, **30**, 325 (1974).
(25) W. Freyland, H. P. Pfeiffer, and F. Hensel, "Proceedings of the Fifth International Conference on Amorphous and Liquid Semiconductors", Taylor and Francis, London, 1974.
(26) J. C. Thompson, *Rev. Mod. Phys.*, **40**, 704 (1968).
(27) J. C. Thompson, ref 49, p 231.
(28) C. A. Kraus, *J. Am. Chem. Soc.*, **43**, 741 (1921).
(29) C. A. Kraus and W. W. Lucasse, *J. Am. Chem. Soc.*, **43**, 2529 (1921).
(30) G. Lepoutre and J. P. Lelieur, ref 2, p 369.
(31) G. Lepoutre, ref 3, p 193.
(32) D. S. Kyser and J. C. Thompson, *J. Chem. Phys.*, **42**, 3910 (1965).
(33) R. D. Nasby and J. C. Thompson, *J. Chem. Phys.*, **53**, 109 (1970).
(34) J. A. Vanderhoff and J. C. Thompson, *J. Chem. Phys.*, **55**, 105 (1971).
(35) R. D. Nasby and J. C. Thompson, *J. Chem. Phys.*, **49**, 969 (1968).
(36) J. A. Morgan, J. A. Schroeder, and J. C. Thompson, *J. Chem. Phys.*, **43**, 4494 (1965).
(37) R. L. Schroeder, J. C. Thompson, and P. L. Oertel, *Phys. Rev.*, **178**, 298 (1969).
(38) J. Castel, J. P. Lelieur, and G. Lepoutre, *J. Phys. (Paris)*, **32**, 211 (1971).
(39) J. P. Lelieur, Ph.D. Thesis, Lille, 1972.
(40) J. P. Lelieur, ref 2b, p 305.
(41) J. P. Lelieur and P. Rigny, *J. Chem. Phys.*, **59**, 1142 (1974).
(42) J. P. Lelieur, *J. Chem. Phys.*, **59**, 1148 (1974).
(43) P. G. Varlashkin and J. C. Thompson, *J. Chem. Phys.*, **38**, 1904 (1963).
(44) J. F. Dewald and G. Lepoutre, *J. Am. Chem. Soc.*, **76**, 3369 (1954); **78**, 2956 (1956).
(45) J. P. Lelieur, P. Damey, and G. Lepoutre, ref 47, p 203.
(46) T. A. Beckman and K. S. Pitzer, *J. Phys. Chem.*, **65**, 1527 (1961).
(47) W. T. Cromenweth and J. C. Thompson, *Adv. Phys.*, **16**, 439 (1967).
(48) R. B. Samoans and J. C. Thompson, *Phys. Rev. A*, **1**, 376 (1970).
(49) N. F. Mott, *Proc. Phys. Soc., Ser. A*, **62**, 416 (1949).
(50) N. F. Mott, *Adv. Phys.*, **16**, 49 (1967).
(51) N. F. Mott, *Phil. Mag.*, **17**, 1259 (1966).
(52) N. F. Mott, *Phil. Mag.*, **17**, 1015 (1972).
(53) N. F. Mott, *Phil. Mag.*, **24**, 1 (1971).
(54) N. F. Mott, *Phil. Mag.*, **19**, 835 (1969).
(55) N. F. Mott, *Phil. Mag.*, **29**, 613 (1974).
(56) N. F. Mott, *Phil. Mag.*, **31**, 217 (1975).
(57) N. F. Mott, *Phys. Rev. Lett.*, **31**, 466 (1973).
(58) M. H. Cohen and J. Jortner, *Phys. Rev. Lett.*, **30**, 699 (1973).
(59) M. H. Cohen and J. Jortner, *Phys. Rev. A*, **10**, 978 (1974).
(60) J. Jortner and M. H. Cohen, *J. Chem. Phys.*, **58**, 5170 (1973); and submitted for publication.
(61) M. H. Cohen and J. Jortner, "Proceedings of the Fifth International Conference on Amorphous and Liquid Semiconductors", Taylor and Francis, London, 1974, p 167.
(62) M. H. Cohen and J. Jortner, *J. Phys. (Paris)*, **35**, C4-345 (1974).
(63) I. Webman, M. H. Cohen, and J. Jortner, submitted to *Phys. Rev.*
(64) (a) J. M. Ziman, *Phil. Mag.*, **6**, 1013 (1961); (b) *Adv. Phys.*, **16**, 578 (1967).
(65) T. E. Faber, *Adv. Phys.*, **15**, 547 (1966).
(66) H. Fukuyama, H. Ebisawa, and J. Wada, *Prof. Theor. Phys.*, **42**, 497 (1968).
(67) L. Ballentine, to be submitted for publication.
(68) A. F. Ioffe and A. R. Regel, *Profiles Semiconductors*, **4**, 237 (1960).
(69) M. H. Cohen, *J. Non-Cryst. Solids*, **4**, 391 (1970).
(70) L. Friedman, *J. Non-Cryst. Solids*, **6**, 329 (1971).
(71) U. Even and J. Jortner, *Phys. Rev. B*, **8**, 2536 (1973).

(72) C. Varea de Alvarez and J. Keller, to be submitted for publication.
(73) M. H. Cohen, H. Fritzsche, and S. R. Ovshinsky, *Phys. Rev. Lett.*, **22**, 1065 (1969).
(74) M. Cutler and N. F. Mott, *Phys. Rev.*, **181**, 1330 (1969).
(75) V. Ambegaokar, B. I. Halpern, and J. S. Langer, *Phys. Rev. B*, **4**, 2612 (1971).
(76) W. Brenig, "Proceedings of the Fifth International Conference on Amorphous and Liquid Semiconductors", Taylor and Francis, London, 1974, p 31.
(77) V. El-Hamany and W. W. Warren, *Phys. Rev. Lett.*, **34**, 1276 (1975).
(78) (a) G. Lepoutre and J. P. Lelieur, ref 2b, p 369; (b) G. Lepoutre, ref 3, p 193.
(79) J. C. Thompson, ref 2a, p 307.
(80) N. W. Ashcroft and G. Russakoff, *Phys. Rev. A*, **1**, 39 (1970).
(81) R. L. Schraeder and J. C. Thompson, *Phys. Rev.*, **179**, 124 (1971).
(82) D. A. Copeland, N. R. Kestner, and J. Jortner, *J. Chem. Phys.*, **53**, 1189 (1970).
(83) J. C. Thompson and K. Ichikawa, *J. Chem. Phys.*, **59**, 1680 (1973).
(84) J. P. Lelieur and P. Rigny, *J. Chem. Phys.*, **59**, 1142 (1973).
(85) J. C. Thompson and J. P. Lelieur, *J. Phys. (Paris)*, **35**, C4-371 (1974).
(86) R. Turner, *J. Phys. F*, **3**, L57 (1973).
(87) P. W. Schmidt, *J. Chem. Phys.*, **27**, 23 (1957).
(88) P. Chieux, *Phys. Lett. A*, in press.
(89) (a) D. E. Bowen, *Phys. Lett.*, in press; (b) P. J. Sams, J. E. Rassing, and E. Wyn-Jones, *Adv. Mol. Relaxation Processes*, **6**, 255 (1975).
(90) H. Weyl, *Math. Ann.*, **71**, 441 (1912).
(91) M. H. Cohen and J. Sak, *J. Non-Cryst. Solids*, **8–10**, 696 (1972).
(92) D. A. G. Bruggeman, *Ann. Phys. (Leipzig)*, **24**, 636 (1935).
(93) V. I. Odelevskii, *J. Tech. Phys. (USSR)*, **21**, 678 (1951).
(94) R. Landauer, *J. Appl. Phys.*, **23**, 779 (1952).
(95) H. J. Juretschki, R. Landauer, and J. A. Swanson, *J. Appl. Phys.*, **27**, 838 (1956).
(96) T. P. Eggarter, *Phys. Rev. A*, **5**, 2496 (1972).
(97) M. H. Cohen and J. Jortner, *Phys. Rev. Lett.*, **30**, 696 (1973).
(98) M. H. Cohen and J. Jortner, to be submitted for publication.
(99) M. H. Cohen, I. Webman, and J. Jortner, to be submitted for publication.
(100) M. H. Cohen and J. Jortner, to be submitted for publication.
(101) D. E. Bowen, ref 2b, p 355.
(102) D. E. Bowen, private communication.
(103) D. W. Mehaffy and D. A. Jerde, *Rev. Mod. Phys.*, **40**, 710 (1968).

Discussion

G. LEPOUTRE. What would be the crucial experiment which would discriminate between the bimodal and unimodal models?

J. JORTNER. Structural data such as those of Chieux, but at smaller angles.

S. O. NIELSEN. Could you elaborate on the tunneling correction to your model and its dependence on b?

J. JORTNER. The validity of our physical picture of a continuous metal–nonmetal transition via the inhomogeneous transport regime was challenged by Mott, who argued that tunneling effects will erode local electronic structure and local transport properties. Indeed, if tunneling effects across nonmetallic regions were important, the local nonmetallic conductivity would be shortened by tunneling and the quantitative details in our theory would be wrong. We have advanced two complementary treatments of the tunneling problem. First, we have demonstrated that for a disordered model system characterized either by large potential fluctuation or by a large correlation length b, tunneling effects are negligible. In this context we have treated an electron in the field of a Gaussian distribution of local potentials [M. H. Cohen and J. Jortner, *J. Phys.*, **35**, C4-345 (1974)]. Tunneling corrections are negligible provided that

$$(b/\text{Å})(\zeta/\text{eV})^2 > 4 \qquad (1)$$

where ζ^2 is the rms of the potential fluctuations. Thus for $\zeta = 0.1$ eV tunneling effects can be disregarded provided that $b > 6$ Å, while for larger potential fluctuations the correlation length which satisfies eq 1 is even smaller. Second, we have explicitly considered tunneling corrections for the specific systems treated by us in detail. In that process we have utilized the values of b extracted from the analysis of the transport data and found that tunneling effects are indeed negligible. We assert that Mott's objection to our approach can be refuted.

The Metal–Insulator Transition in Metal–Ammonia Solutions

N. F. Mott

Cavendish Laboratory, University of Cambridge, Cambridge, England

Publication costs assisted by Cavendish Laboratory

An outline of our present knowledge of the behavior of the electrical properties of noncrystalline systems is given, and an attempt is made to apply it to metal–ammonia solutions. The solubility gap in metal–ammonia is, we believe, a direct and necessary consequence of any metal–insulator transition of band-crossing or Mott type; but above the consolute temperature the transition becomes of the Anderson type. In the range of concentration where d log $\sigma/\mathrm{d}T$ is large, an extra electron is thought to jump from one diamagnetic pair to another. A model is proposed in which the activation energy is partly of polaron type.

Metal-insulator transitions have now been studied in many noncrystalline systems, and it seems to the present author that, in spite of some unsolved problems relating for instance to the Hall effect, enough theoretical and experimental information is available to give us a fair idea of how such systems behave. Among these noncrystalline systems metal–ammonia solutions are perhaps the most complicated. The available experimental information is exceptionally extensive, but to interpret it the theory of electrons moving in a rigid noncrystalline medium may be insufficient, because the electrons themselves create their own environment. It was first shown by Jortner[1] that, for low concentrations of metal, each electron is trapped in a cavity of its own creation, the surrounding ammonia being polarized. For the interpretation of the metal-insulator transition, it may be necessary to assume that moving electrons carry